UNIVERSITA' DEGLI STUDI DI NAPOLI FEDERICO II

Scuola Politecnica e delle Scienze di Base
Corso di Laurea Magistrale in Ingegneria Informatica

Tesi di Laurea Magistrale in Misure su Reti di Comunicazione

Metrological characterization of field markers for real-time measurement and control of accelerator magnets

Anno Accademico 2016/2017

Relatore

Ch.mo Prof. Pasquale Arpaia

Correlatore

Dott. Ing. Marco Buzio

Candidato

Maria Amodeo

Matr. M63000597

Alla mia famiglia.

Contents

List of Figures

List of Tables

Introduction

In synchrotrons, knowledge of the integrated field of the bending dipoles is essential for transversal and longitudinal beam control. In some special cases, such as the conductor-dominated, very high-field LHC superconducting dipoles, the field can be predicted accurately enough by means of semi-empirical mathematical models [1]. In general though, especially in the case of iron-dominated magnets, precise prediction of non-linear and dynamic effects is beyond the current state-of-the-art. While a number of well-established techniques exist to improve reproducibility (for example, by pre-cycling) and to stabilize the field on flat-tops (for example, by applying current overshoots), these are often too costly in terms of lost beam time. In such cases, feedback control based on magnetic field measurements is therefore a necessity.

At CERN, five so-called "*B-train*" systems are used to measure in real time the field of a reference magnet, which can be either one of those in the ring or an additional unit, installed in a separated facility and excited in series with the ring [2]. The "train" moniker derives from the distribution of B, which is commonly based on two trains of digital pulses representing fixed 0.1 G increments or decrements of the field. Typical users of the measured field include: the RF accelerating cavities and the main dipole power supplies; certain beam diagnostics, such as the beam current DCCT (Direct Current-to-Current Transformer), which uses it to normalize with respect to the relativistic velocity; and, of course, the operation team in the control room.

In essence, these systems measure the field B according to the Equation 1:

$$B(t) = B_0 + K \int_0^t V_c(\tau)\, d\tau \tag{1}$$

where V_c is the voltage output of an induction coil, the coefficient K has the physical dimensions of m^{-2}, and the integration constant (B_0) is either a preset value, or it is obtained from an additional sensor, generally called a field marker.

A coil is the generally preferred method of measuring the dynamic part because it is linear, it can be relatively easy to calibrate precisely, and it can measure also the average field of very long magnet. As it is well, known, the main problem associated to integration is drift due to offset at the integrator input. In the B-train systems currently in operation at CERN, this is kept at a level about 50-100 uT/s which has been historically considered adequate. However, upcoming accelerators will need not only a generally higher level of accuracy, but also the integration to be protracted for very long durations.

Currently a new generation of B-train systems is being developed and tested at CERN in the frame of a complex-wide consolidation project, with the specific purpose to improve their performance and guarantee their long-term maintainability. These new systems will need a new and better drift correction strategies, especially in the case of field plateaux up to two minutes long. In particular, the goal of this thesis is to study the performance of a new teslameter as a so-called field marker for the correction of the drift under such conditions.

Chapter 1 introduces the CERN accelerator complex and provides a full overview of the state-of-the-art in literature about sensors used to measure magnetic field and correction techniques for flux integrator, also explaining the motivation of the choices made on the sensors to be used.

Chapter 2 focuses on the measurement model and the new technique proposed for drift correction.

In Chapter 3 there is a description of the teslameter chosen to measure field values.

Chapter 4 shows the experimental results obtained in the case of a DC field source and, finally, the conclusion are reported in Chapter 5.

Chapter 1

Overview

1.1 Context

What is CERN? *The European Organization for Nuclear Research*, known as CERN, is one of the world's greatest and most prestigious laboratories.

The main goal of physicists and engineers is the study of high-energy physics. In order to understand the fundamental structure of matter, which is linked to the evolution of the Universe just after the Big Bang, the particles are made to collide together at very high speed, close to the speed of light.

Established in 1954, the organization is situated on the Franco-Swiss border and has 22 member states. Thanks to these international collaborations, it was possible to realize special particle accelerators and detectors, needed for high-energy physics research. Accelerators allow beams to reach high energies; after that the beams are made to collide, the energy liberated by the collision gives rise to new particles which are analyzed in large detectors. The *Large Hadron Collider*(LHC) is the world's most powerful accelerator; it is a ring of 27 km circumference in which protons or heavy ions (e.g. lead) circulate at close to the speed of light and these particles are called hadrons. There are several hundreds of millions of collisions every seconds that recreate the conditions of the first moments of the universe and produce billions of new particles, a small fraction of which is of scientific interest. A wide network of computers filters, records and processes the data from the collisions and the CERN computing grid distributes worldwide and processes 30 PB of data each year. In July 2012, the ATLAS and CMS experiments at CERN's LHC led to the discovery of a new particle: the *Higgs boson*, the last one predicted by the Standard Model but not found for 40 years.

It is important to remember that in order to build these accelerator and detector, it is necessary to further advance in many areas of technology; in fact the technologies developed for particle physics research also benefit many sectors of industry and medicine.

As a striking example, CERN is also the birthplace of the *World Wide Web*; it was invented by Tim Berners-Lee, a British scientist, in order to allow the sharing of particle collision data between scientists in universities around the world.

1.2 The accelerator complex

The accelerator complex at CERN, represented in Fig. 1.1, includes eleven machines that accelerate particles in order to increase their energy; in fact, each machine in the chain increases the energy of the particles by a factor typically around 20 limited by non-linearities, before delivering them to the next more powerful accelerator or to experiments. There are four main experiments in the LHC (CMS, ATLAS, LHCb and ALICE) and dozen of smaller experiments (LHC or fixed-target); each of them studies particle collisions from a different aspect and with different technologies.

Let us start by considering the chain of injectors delivering protons to the LHC. The proton source is a simple bottle of hydrogen gas and an electric field is used to separate electrons from hydrogen atoms in order to have protons (*ionization*).

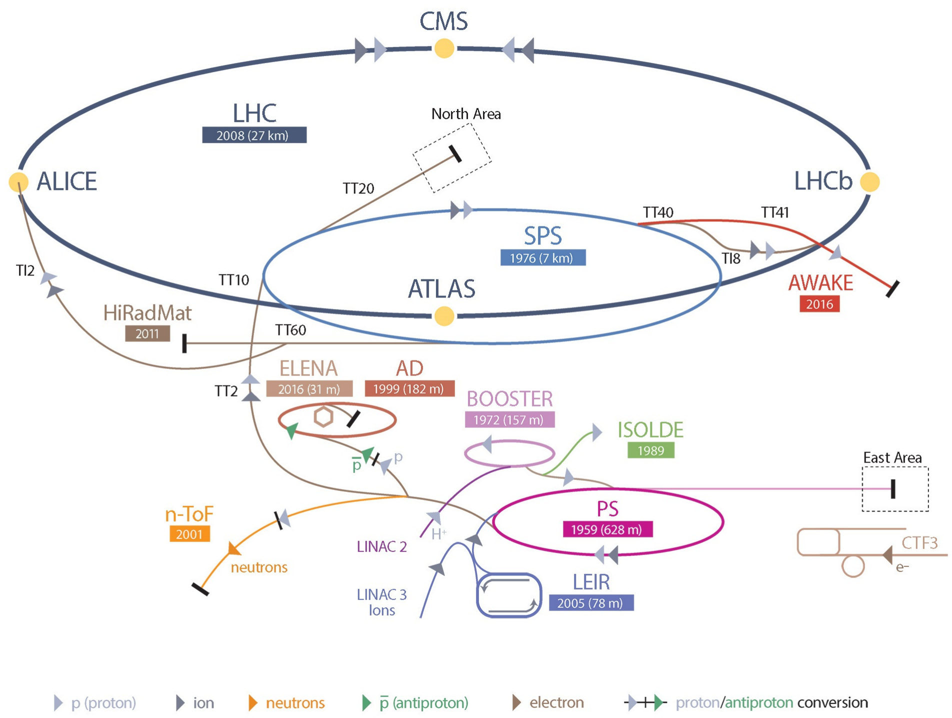

Figure 1.1: CERN's Accelerator Complex

The first accelerator in the chain is LINAC 2. LINAC 2 accelerates protons to 50 MeV, while the Proton Synchrotron Booster accelerates the protons to 1.4 GeV. The latter injects the beam into the Proton Synchrotron (PS) that accelerates the protons to the energy of 26 GeV. Finally, they are sent to the Super Proton Synchrotron (SPS) with an energy of 450 GeV and then in the Large Hadron Collider (LHC), where an energy of 6.5 TeV per beam is reached today.

In the LHC, two beams circulate in opposite directions in order to collide inside four detectors, where the center-of-mass energy at the collision point is equal to 13 TeV.

It is noteworthy that, besides the protons, it is possible to accelerate ions of various types too. For example, a source of vaporized lead produces lead ions; they enter first LINAC 3, they are injected into the Low Energy Ion Ring (LEIR) which accelerates the ions from the ion linear accelerator in order to transfer them to the Proton Synchrotron (PS). The route then continues as in the case of protons.

All the circular machines in the complex are synchrotrons. A **synchrotron** is a cyclic particle accelerator and the particle beam is accelerated around a fixed closed-loop path. The magnetic field guides the beam along the ring and increases during acceleration, in order to maintain a constant radius. It is extremely important therefore to know very precisely the magnetic field at all times, so that the beam may remain stable and well-centered on its theoretical orbit during the injection, acceleration and extraction phases.

A sophisticated timing system is necessary in order to synchronize the accelerators. We talk about beam scheduling to decide which beam to produce in a given accelerator at a given time [3]. The machines work with cycles of different nature that go to different users. The cycles are organized in supercycles that are repeated during the day, so a *supercycle* can be seen as a *cycle of cycles*. Moreover, it is important to consider that each accelerator requires a different time to produce a beam; so the schedule of the beams is a task as complex as essential to operate the entire chain correctly.

We shall now describe in some detail the accelerators that are the objective of this thesis, paying attention in particular to the characteristics of their magnetic cycles.

1.2.1 Proton Synchrotron Booster - PSB

The **Proton Synchrotron Booster** (1972) is the first circular proton accelerator in the chain and receives the beams from LINAC 2. It has the peculiarity that four rings are arranged one above the other. This has the advantage that more particles can be accelerated at the same time, reaching 1.4 GeV for injection into the Proton Synchrotron (PS).

The field level from injection to extraction goes from 0.125 T to 0.861 T, while the duration of the cycle is 1.2 s. There is a limited variety of cycles, which helps the magnetic reproducibility of the machine.

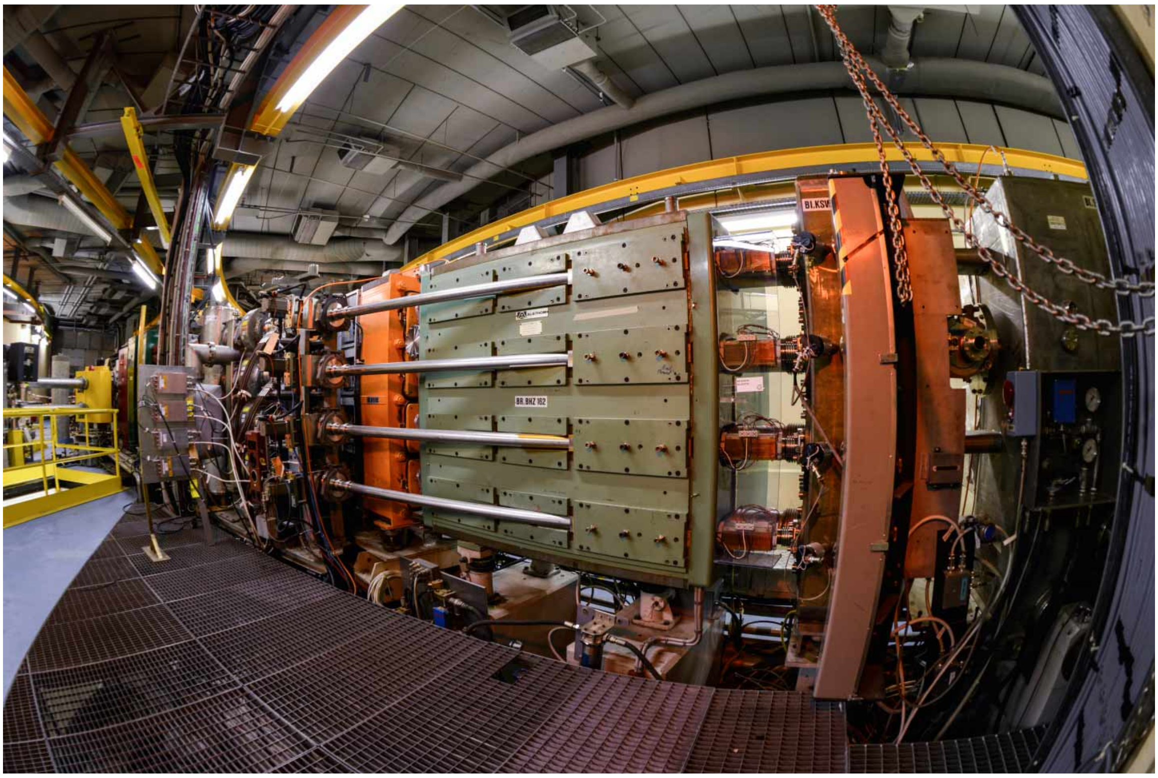

Figure 1.2: Proton Synchrotron Booster- PSB

1.2.2 Proton Synchrotron - PS

The **Proton Synchrotron**, which began working in 1959, is CERN's first synchrotron. It is used both to speed up protons coming from the PSB and heavy ions coming from the LEIR. Until the 70s, it was the protagonist within CERN, but later other accelerators were made. In addition to being a part of the LHC injector chain, the PS also provides beam to a number of smaller fixed-target nuclear physics experiments in CERN's East Area.

The PS has a circumference of 628 meters and it has 100 dipoles to direct the beam along the ring path. The field level from injection to extraction goes from 0.1 T to 1.26 T, while the duration of the cycle can be a multiple of 1.2 s (1.2 s, 2.4 s, 3.6 s). There are many type of different cycles that create magnetic hysteresis and, for this reason, field is impossible to predict but must be measured.

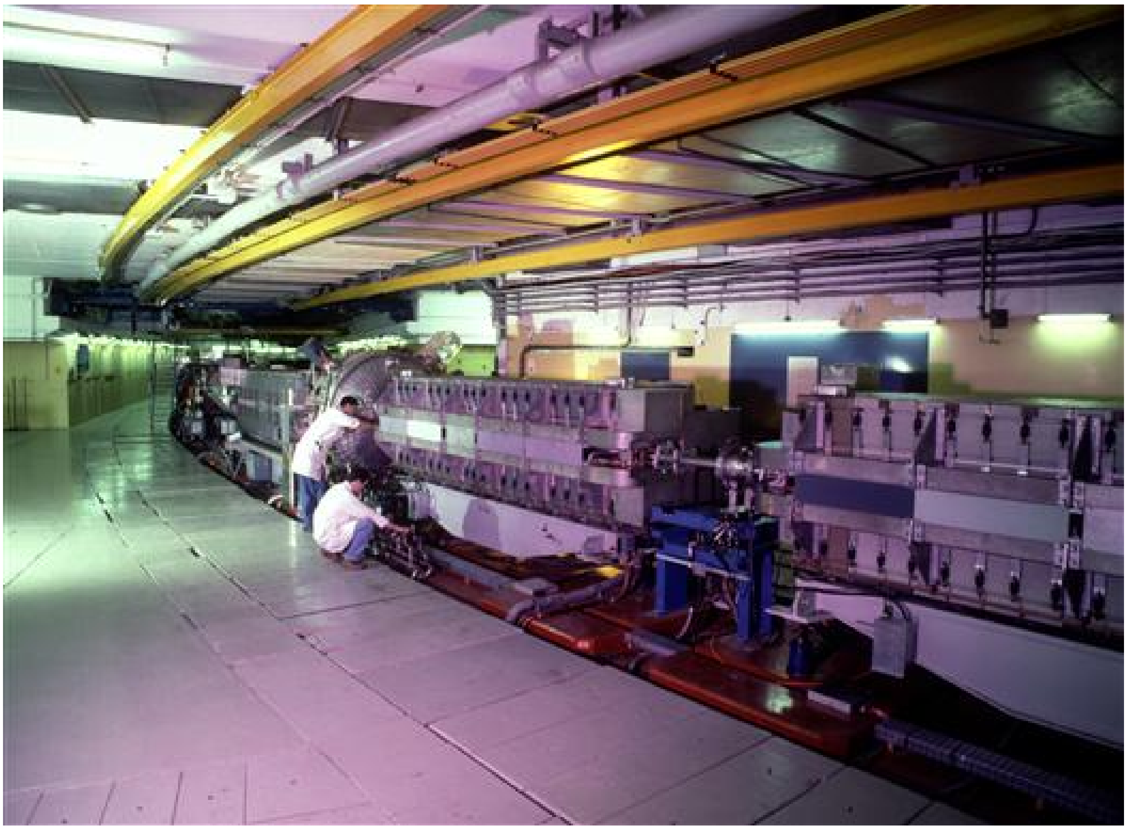

Figure 1.3: Proton Synchrotron - PS

1.2.3 Super Proton Synchrotron - SPS

The **Super Proton Synchrotron** is the next stage of the accelerator chain. It has a circumference of 6.9 km and allows the passage of particles from the PS to the LHC. Moreover, it provides the beams for several fixed target experiments, such as NA61/SHINE, NA62 and COMPASS. It consists of 1317 conventional electromagnets and accelerates different types of particles such as protons and ions. It operates from 1976 and the main discoveries were the W and Z bosons in the UA1 and UA2 experiments, which lead to the assignment of the Nobel Prize to Carlo Rubbia and his team. Today, the SPS accelerates particles up to 450 GeV and from 2006 to 2012, the CNGS experiment used it to produce a neutrino beam in order to detect it at the Gran Sasso laboratory, in Italy.
The field in SPS dipoles reaches a high level of 2.02 T, while the cycles are widely different according to the experiments and can be as long as around 30 s in case of slow extraction to certain fixed-target experiments that require a steady particle influx, rather than the more common discontinuous bunches. This process is based on the purposeful excitation of resonant instabilities in the beam, hence its needs very precise measurement and control of magnetic field [4].

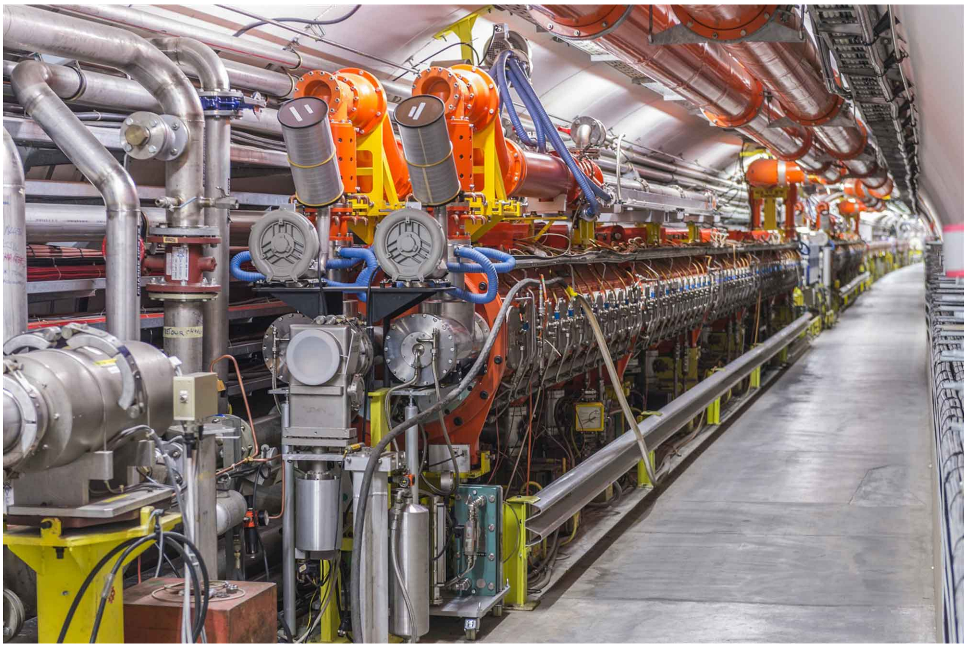

Figure 1.4: Super Proton Synchrotron - SPS

1.2.4 Low Energy Ion Ring - LEIR

The **Low Energy Ion Ring** is the second step in the ion accelerator chain, after LINAC 3. It is a conversion from the old Low-Energy Antiproton Ring (LEAR), used to decelerate antiprotons and to deliver them to experiments. LEIR was first proposed in 1993 and, after a period of updating, since 2010 it is able to provide ions for collisions within the LHC. Regarding the operation, it receives long bunches of ions from LINAC 3 and splits them into four shorter bunches; then it accelerates these bunches up to 72 MeV in order to pass them to the PS. Since the LEIR takes 2.4 s to accelerate the bunches, in groups of two, and LHC uses 592 bunches of ions per beam, it will take about 10 minutes for LEIR to allow the complete filling of the LHC.
LEIR has only four bendling dipoles, with a very strong 90° curvature, reaching up to 1.15 T. Like the PS, cycle length can be 1.2 s, 2.4 s and 3.6 s, however only one type of cycle is predominantly played during any given year-long run.

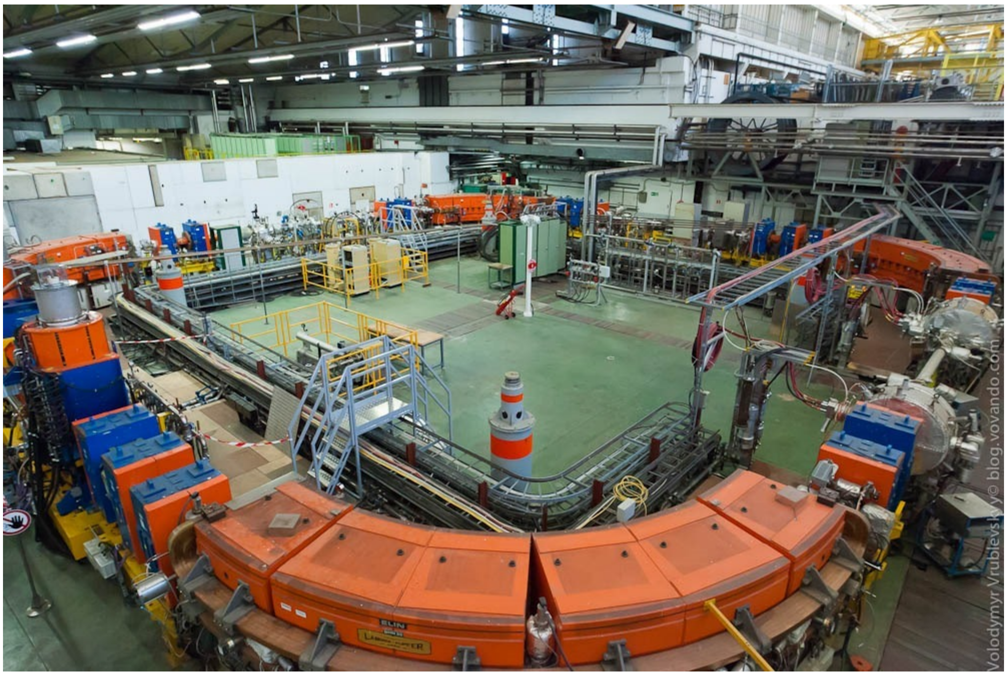

Figure 1.5: Low Energy Ion Ring - LEIR

1.2.5 Antiproton Decelerator - AD

In this accelerator complex, there are also the Antiproton Decelerator (AD) and ELENA, which produces low-energy antiprotons for studies of antimatter, and the Online Isotope Mass Separator (ISOLDE) facility, which is used to produce and study unstable nuclei.

The **Antiproton Decelerator** is a machine downstream of the PS that produces antiprotons and sends them to the various experiments, for studies of antimatter. The antiprotons, created by the collision of the proton beam with a block of metal, must be decelerated to an energy of 5.3 MeV, by strong electric fields, in order to produce antiatoms. Then, they are sent to the different experiments. The AD was installed in 2000 and it made headlines when, for the first time, antihydrogen atoms were produced and trapped. Since 2010, thanks to the AD experiments, there were numerous measurements of antimatter characteristics. Among the various experiments, we remember ALPHA (it makes, captures and studies atoms of antihydrogen and compares them with hydrogen atoms [5]), ASACUSA (it compares matter and antimatter using atoms of antiprotonic helium and antihydrogen, and studies the properties of matter-antimatter collisions [6]), ATRAP (it compares hydrogen atoms with their antimatter equivalents - antihydrogen atoms [7]) and BASE (it compares matter with antimatter, making the most precise measurements of the magnetic moments of protons and antiprotons [8]).

Figure 1.6: Antiproton Decelerator - AD

The magnetic cycle in the AD is only of one type and for this reason it is extremely reproducible, so that a measurement is not necessary. A B-train system is operational, although it transmits a static image of the reference magnetic cycle, which has been found to be adequate for the machine to function.

1.2.6 Extra Low ENergy Antiproton - ELENA

The **Extra Low ENergy Antiproton** ring is a new hexagonal deceleration ring located in the AD complex. It has a circumference of 30 meters and, activated in 2016, it is realized to further decelerate the antiproton beam from 5.3 MeV to an energy of 0.1 MeV, in order to allow more precise measurements. Thanks to an electron cooling system, it will be possible to increase the beam density, improving the efficiency of the experiments by three orders of magnitude. GBAR, aiming at measuring the velocity at which antihydrogen atoms fall in the Earth's gravity, will be the first experiment to use a beam prepared by ELENA.
The field is very low, from 0.05 T to 0.42 T, while the cycle duration is very long, up to two minutes, in order to allow the cooling effect of the electron beam. The combination of these two factors make precise control and measurement of the magnetic field extremely challenging, especially because at low energy the beam is very sensitive to the smallest field perturbations.

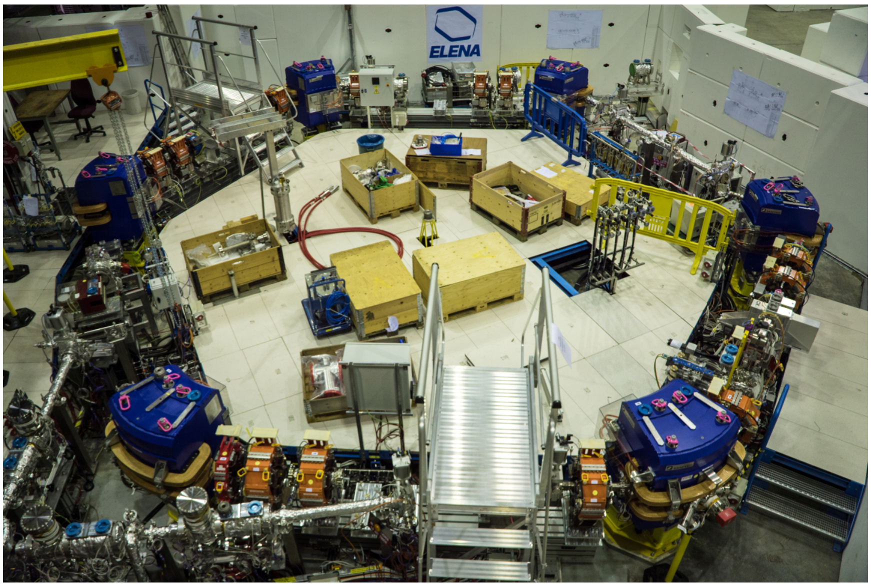

Figure 1.7: Extra Low ENergy Antiproton - ELENA

1.2.7 Accelerators for medical purpose - CNAO

Synchrotrons are used not only for high energy physics research, but can also be used for medical purposes as in the case of the *National Centre for Oncological Hadrontherapy* (CNAO), that is a hospital center dedicated to the treatment of tumors by hadrontherapy. It was inaugurated in Pavia on 15 February, 2010 with the aim of curing patients suffering from solid tumors by using proton beams and carbon ions. CERN participated in the construction of the CNAO accelerator complex where, in dedicated areas of the facility, radiobiological and clinical research are also performed.
The accelerator complex consists of 2 ion sources, a 7 MeV/u injector, a 78 m long synchrotron and 4 extraction lines. The magnetic bending in the synchrotron is realized by 16 dipoles [9]. The beams of protons are accelerated up 250 MeV, while beams of carbon ions are accelerated up to 400 MeV/u. This particular therapy may be useful for treating radio-resistant or inoperable tumors. Since it is possible to direct beams of protons or ions precisely, the hadrontherapy is also suitable for treating deep-seated tumors or those critical because of the position close to the vital organs. For example, the survival rate for chondrosarcomas at 15 years goes from 5% to 95%.
To do so requires the beam position to be controlled with a precision of about 0.1 mm. In addition, the beam energy is related to the penetration of the beam inside the body, so that it must be changed rapidly and accurately in order to deposit energy in a controlled way at different depths (this technique is called ”3D painting”). This means that real-time measurement of the bending magnetic field is particularly critical in this class of machines. For this reason, a B-Train system has been realized and it is similar to the B-Train system for the PS at CERN. The goal of this control system is to provide a real-time measurement of the magnetic field of the bending dipoles and this measurement is used to produce a feedback correction signal for the dipoles Power Supply.

1.3 State-of-the-art of magnetic field sensors

The real-time knowledge of the magnetic field, used in order to bend and focus the beam, is of fundamental importance, inside the particle accelerators [10]. This information is used by different subsystems, such as RF cavities and beam control, as feedback in the control system. There are two different ways to acquire field values in real time: through magnetic measurement systems or through mathematical models of the magnet response. In the first case, the measurements are typically carried out in a reference magnet (powered in series with the accelerator magnet chain) and then data are distributed to the various subsystems through the so-called *B-Train*, i.e. two parallel incremental and decremental digital pulse trains. In this way, each user can get the field value as a function of time counting the impulses.

B-trains are operational since inception in LEIR, PSB, PS, SPS and AD [11]; a completely new system is being developed for ELENA [12]. All include a facility, known as "simulated" or "synthetic" B-train, which distributes an image of the nominal cycle as stored in LSA and that, under certain circumstances, can complement or replace the measurement. In all cases, the B-train is absolutely essential for each of these accelerators to function.

The coil fluxmeter meets all the requirements in terms of precision, accuracy and response time but a further measurement is necessary to acquire the field value to be used as integration constant. Typically, for this purpose the so-called *"field markers"* are used, i.e. measurement systems capable of providing a digital pulse when the field crosses a certain threshold. An alternative to the coil fluxmeter would be the Hall probe, but at CERN the Hall probes were considered too noisy and not sufficiently precise for this type of application.

1.3.1 Magnetic field sensors

The most commonly used magnetic measurement techniques are:

- Induction coil;
- Peaking strips;
- Nuclear Magnetic Resonance (NMR);
- Ferrimagnetic Resonance (FMR);
- Hall Probes.

Several factors affect the choice of a measurement method, such as the field strength, variation in time (bandwidth) and tolerance to spatial gradients, as well as the required accuracy.

Coil

A generic **coil** works according to *Faraday's law.* When the magnetic field concatenated with a coil changes, an electromotive force appears in the coil itself, called *induced electromotive force (emf)*:

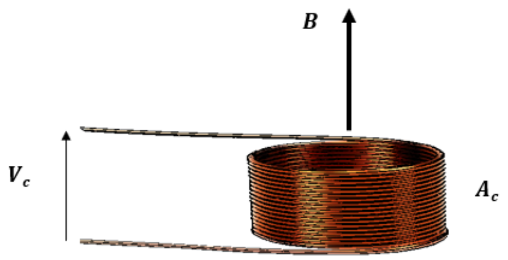

Figure 1.8: Coil

$$V_c = -\frac{d\Phi}{dt} + V_0 \qquad \textit{Faraday-Neumann's law} \tag{1.1}$$

where Φ is the magnetic flux.

The induced emf is equal to the rate of change of the linked flux; in addition, emf it is negative when the flux increases and positive when it decreases. If flux unit is $T \cdot m^2$ (Weber) and time unit is second, then emf unit is Volt.

The variation of the magnetic field can occur for different reasons: change of magnetic field strength, magnet displacement to or away from coil, coil displacement in or out of magnetic field, coil rotation relative to the magnet, etc.

The *fluxmeter method* is the oldest used methods for magnetic measurements and it can be very precise. This method has been chosen for the timing-changing part of the field and accuracy is given by the calibration accuracy of the coil. The main source of error is given by the voltage offset V_0, which is due to various causes including thermocouple voltages along the cabling, electronic component imbalance and rectification of electrical noise.

Peaking strips

The term **peaking strip** indicates a device used to measure dynamic magnetic fields (it is a dynamic marker), with an accuracy of approximately ±0.02 G [13]. With this instrument it is possible to measure magnetic fields up to several hundred Gauss with air-cooled bias coils, while in order to measure field of the order of kilogauss it is necessary to use water-cooled bias coils. It is composed by a ferromagnetic strip with high permeability and different types of coil. Peaking strips are extremely stable and reliable in time and magnetic measurement process is simple. Despite these advantages, there are several reasons why they have been used less and less over time. In particular, it works when the magnetic field is low and it is difficult to make a new strips and to maintain existing ones.

Nuclear Magnetic Resonance - NMR

Today, the **NMR**, experimentally demonstrated in 1945, is the most accurate method for measuring magnetic field strength, able to reach an accuracy of parts per million (10^{-6}). NMR magnetometers are mostly used as a reference to calibrate others but the field of use is destined to become wider, while in medicine *Magnetic Resonance Imaging* (MRI) has spread and has become one of the most important imaging techniques. The operating principle [14] of an NMR magnetometer will be explained below.

NMR is a physical phenomenon based on the fact that the protons and neutrons possess a magnetic dipole moment, that is they are equivalent to microscopic bar magnets. This moment, which is positive for protons and negative for neutrons, is analogous to the magnetic moment created by an electric charge rotating around its axis and is described in quantum mechanics by the property called *spin*, which for an isolated particle can take only two equal and opposite values. Resonance can occur when the nuclei of certain atoms are immersed in a static magnetic field (B_0) and are exposed to a second oscillating magnetic field (B_1). Some atoms experience this phenomenon, while others never experience it and this depends on the net moment of the nucleus, which is the algebraic sum of the moments of the constituent protons and neutrons (a non-zero moment requires an odd number of protons, or neutrons, or both). Among the many elements with spin, the most commonly measured nuclei are hydrogen-1 (also chosen as the element with which to produce MR imaging since it is the simplest and most abundant element in the human body) and carbon-13. Normally, these microscopic magnetic fields are randomly oriented and, therefore, the magnetic vector resulting from their sum is zero. If subjected to a strong stationary external magnetic field (B_0), the proton axis will orient itself along the field itself. This orientation can take place either in the same direction as B_0 (i.e with a low energy level) or in the opposite direction (i.e. with a high energy level). The difference between these two energy levels depends only on the magnetic moment and the magnetic field, as shown in Fig. 1.9. The nuclear magnetic moment is a constant, so this energy gap is a precise measure of magnetic field strength.

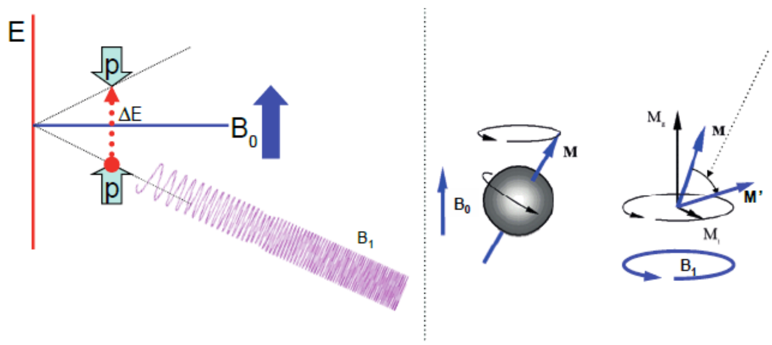

Figure 1.9: Energy level transition (quantum view) and spin precession (classical view)

The parallel protons are slightly more prevalent than the antiparallel ones. This small prevalence produces a resulting magnetization M, parallel to B_0 and measurable. In the classical view, which describes the phenomenon to a very good degree of approximation, due to the effect of B_0, the axis of each proton rotates around the direction of the moment of B_0 (*precession*). The precession frequency is characteristic of every atomic element and is called *Larmor frequency*. As regards

hydrogen, for example, in order to resonate the Hydrogen protons, a RF field B_1, perpendicular to B_0, is sent with a frequency equal to the frequency of Larmor for Hydrogen.
The resonant frequency is given by the following relation:

$$\nu_{Larmor} = \gamma \cdot B_0 \tag{1.2}$$

where γ is the gyromagnetic ratio, that is the ratio between its magnetic moment and its angular momentum. The gyromagnetic ratio for an isolated proton is 42.57747892 MHz/T. Consequently, resonant frequencies for a particular substance are directly proportional to the strength of the applied magnetic field. The gyromagnetic ratio is known from fundamental constants with an uncertainty lower than 10^{-8}, which is the reason for the accuracy of the method.

At resonance, the nuclei absorb and release energy while flipping back and forth between the two opposite spin states. The disequilibrium between the two populations gives rise to a measurable signal. For a NMR teslameter, there are two basic modes of operation:

- Continuous Wave (CW) the sample is continuously hit by an RF wave while at the same time the background field B_0 is slowly modulated by a superposed field generated by an additional coil, which causes the resonance to be crossed periodically. At resonance, absorption of energy by the sample is detected by a further detection coil;
- Pulsed Wave (PW): a single RF coil is used to send short RF pulses to the sample and to read its response. The amplitude and time decay of the response contain information on the background field.

Pulsed wave is made possible by relatively simple modern electronics and is the preferred method for a teslameter, which can operate following time-changing background fields. NMR represents the metrological standard and for this reason it is used whenever possible, if compatible with the uniformity of the background field since a gradient spreads out the resonance and flattens the peak, thus reducing accuracy.
Given the precision of the method and being interested in working on long-plateaux in this thesis, NMR was chosen as field marker.

Ferrimagnetic Resonance - FMR

The **Ferrimagnetic Resonance** is similar in principle to NMR, but is less precise. FMR is based on the precession of electrons, which happens at a frequency of about 28 GHz/T. This very high frequency range allows clean detection of noise-free signals, however the gyromagnetic ratio is strongly affected by the temperature and chemical composition of the sample, so that the metrological performance is lower than NMR. The problem of this type of sensor is that it can only function as a dynamic marker since a DC implementation is not available in commerce, so it is not suitable for our purpose.

Hall Probes

The **Hall probe** is a device that allows the measurement of the intensity of the magnetic field using the *Hall effect*. Given a bar of semi-conductor (or conductor), crossed by a current i, subjected to a magnetic field B orthogonal to the direction of the current, the Hall effect consists in the formation of an electric potential difference (the Hall voltage) between the ends of the section of the circuit orthogonal to the current. The Hall voltage thus generated is proportional to the known current and to the field.

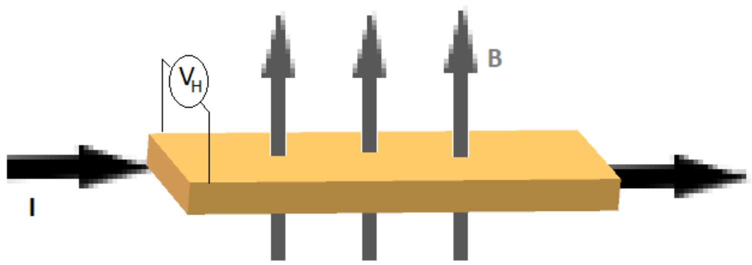

Figure 1.10: Hall Effect

The Hall Probe works both in DC and in time-varying fields and is widely used because the sensor is produced by standard CMOS fabrication technique and is therefore very cheap; it can also detect a large range of fields. The disadvantage is that it is very sensible to the temperature.

1.3.2 State-of-the-art of integrator drift correction

The problem of drift is strongly felt in different fields and the techniques of drift correction are therefore used in many domains, from inertial sensors to magnetic measurements.
Below the techniques used for the correction of drift for the different domains are described.

Drift correction for inertial sensors

In some applications displacements are measured by integrating acceleration rather than through position sensors, for example where displacements are difficult to measure. However, by directly integrating the acceleration signals, drift will appear in the speed and displacement signals.

The reasons why these drifts appear are different, for example offset in acceleration, random noise in acceleration, etc. If *a(t)* is the measured acceleration, the velocity will be given by the following relationship

$$v(t) = v_0 + \int_0^t a(\tau)\, d\tau \tag{1.3}$$

where v_0 represents the initial velocity.

The displacement can be written as:

$$s(t) = s_0 + \int_0^t v(\tau)\, d\tau = s_0 + v_0 t + \int_0^t \int_0^\tau a(\tau)\, d\tau\, dt \tag{1.4}$$

where s_0 represents the initial displacement.

In order to calculate the displacement, it is necessary to know the initial displacement and the initial velocity. If these two terms are null, then it is possible to calculate the displacement from the Equation 1.4. Typically, however, these two terms are not null and this will lead to an integration error in the displacement. Numerical integration is very widespread and there are several discrete integration algorithms; acceleration is first sampled and then integration is done. So even if there are small errors in the measurement, they will result in larger drift in velocity and displacement. Different methods have been proposed to eliminate the phenomenon of drift within speed and displacement; among these solutions, there is the approach in which "drifts are estimated by using the mean of the upper and lower envelopes of signals after integration from acceleration into velocity and displacement" [15]. In particular:

1. the acceleration signal is integrated with a numerical integration method;
2. the upper and lower envelopes of the integrated signal are calculated;
3. the mean of the upper and lower envelopes is calculated to obtain the basic offsets;
4. the mean of the upper and lower envelopes is subtracted from the integrated signal in order to have the velocity signal.

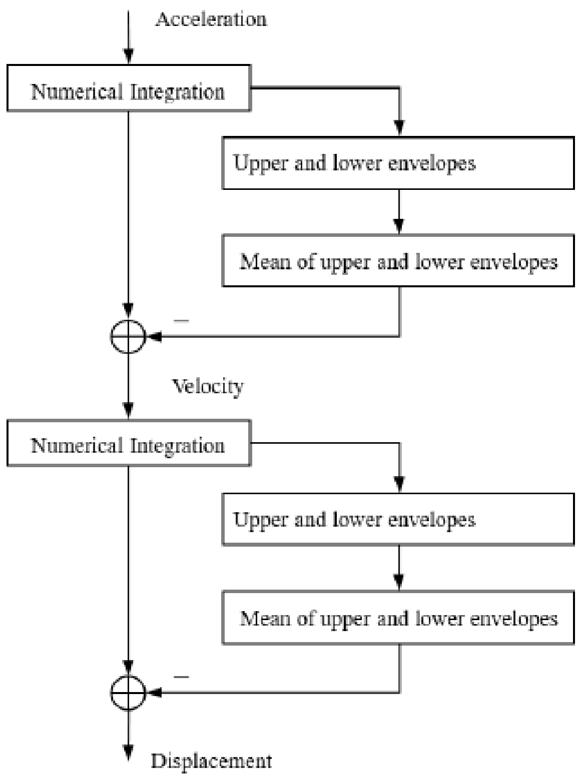

Figure 1.11: Block diagram of envelope method [15]

This method works well in its context because the output of an accelerometer is dominated by high frequency noise, and the mean of the upper and lower envelopes can be assumed to be a spurious offset superimposed to the real signal. Unfortunately, it cannot be applied to the present case since typical voltage offsets evolve only slowly with time.

Drift correction for induction coils for nuclear fusion

Nuclear fusion is the mechanism that powers the sun and the stars and several studies are underway to reproduce it in a controlled way as an energy source [16]. In order to have the fusion between two nuclei it is necessary to overcome the electromagnetic repulsion due to their positive charges. By heating the reagents to a sufficiently high temperature, it is possible to produce the required reactions, the fusion fuel ionizes and forms a plasma. After a fusion reaction there is a loss of mass that is converted into energy.

A **Tokamak** is a machine designed to contain a thermonuclear plasma, thanks to the particular structure of the magnetic field created in it in order to isolate the plasma from the walls of the vacuum toroidal container. The magnetic field is pulsed cyclically up to a level of several tesla, with typical cycle durations that range from a fraction of a second to several seconds or minutes in the largest machines. The magnetic field must be known to a precision below 1% for the whole duration of the cycle in order to derive information on the configuration of the plasma, which leads to measurement systems and problems very similar to those in the context of accelerator magnets. A magnetic diagnostics is composed of inductive coils and integrators and is used to measure the magnetic field strength and flux [17]. Because of the drift due to integration, the analogue integrator can not be used for too long periods (a few minutes). The main techniques adopted were the following: analog integrator based on ADC-register-DAC [18], integrator based on field programmable gate array (FPGA) [19], alternating integrator [20], an integrator consisting of a digital-analog combination of a DSP and an ADC [21].

For new machines, such as ITER, currently being built at Cadarache, France, where there may be integration periods of up to 1000 seconds, the goal to achieve a more advanced integrator design exists. For example, this is the case of EAST, that is a superconducting tokamak experimental device for which a new alternating integrator has been designed. Real-time drift compensation is achieved by a pair of integrator cells that work alternately [17], through the switches configuration which is controlled by an FPGA. In this way, while one cell integrates, the other cell clears the capacitor. Performance tests show that the new designed and developed integrator for EAST has a low offset (< 15 mV) for 1000 s.

Another example of an integrator designed to reduce the phenomenon of drift is the fully digital integrator developed for HL-2A magnetic diagnostics [22]. In this case, a 24-bit ADC and simple analog processing circuits are realized for high-precision sampling, while several correction algorithms are used in order to minimize the drift. Also in this case, the experimental results have shown that the performances relative to the drift satisfy the requirements of HL-2A.

In general, the techniques used in the context of fusion reactors cannot be easily transported to the problem considered here. This is mainly due to the fact that, for accelerator purposes, the field must be known to a far greater degree of accuracy and with a very large bandwidth, up to several hundred of kHz for feedback to the RF system. Electronic chopping or switching techniques often introduce high frequency components that must be filtered out, leading to unacceptable results.

Drift correction for rotating induction coils for accelerator magnets

In particle accelerators, the quality of the magnetic field is of fundamental importance and this is also guaranteed by high quality magnetic measurements. The **rotating coil** method can be used to measure homogeneous or inhomogeneous magnetic fields. According to Faraday's law 1.1, when a conductor loop moves relative to a magnetic field, there will be a variation in flux and a voltage will be induced proportional to the time variation of the flux. Also in this case it is necessary to eliminate the drift effect produced by the integrator.

In the case in which rotating coils are used to perform the field measurement, the signal periodicity can be used to correct the drift phenomenon. In fact, at constant field, the flux change after a full rotation must be zero. This makes possible an effective correction when the rotation time is short, of the order of a second or less.

In the case of long measurements, a new method for drift correction in digital integrators has been proposed [23]. This correction technique is based on the following automatic feedback loop

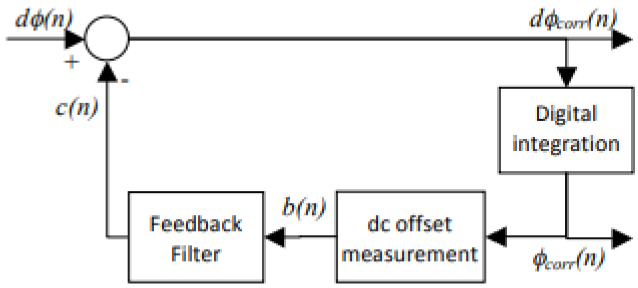

Figure 1.12: Block scheme of feedback loop for drift correction

The operation of the feedback loop is based on the sequence $d\Phi(n)$ of flux increments, measured on a fraction of the period of the rotating coil. At the beginning, the control sequence *c(n)* is null and the magnetic flux $\Phi(n)$ is obtained by integrating the samples $d\Phi(n)$. Then there is the block that calculates the dc offset affecting the flux sequence, that is filtered by a low-pass filter. The control sequence *c(n)* is thus produced and is subtracted from the $d\Phi(n)$ sequence. Experimental tests have shown the ability of this technique to correct the DC offset.

Drift correction for fixed induction coils for accelerator magnets

In the domain of accelerators, measurements of pulsed fields with fixed induction coils are very common both offline, when then magnet is on a test bench for acceptance and qualifications tests, and on-line for B-train systems. In principle, drift correction techniques are similar for both cases, although for B-train the problem is made more difficult by the necessity to estimate and correct the drift in real time. Cycles are of the order of a few seconds up to 120 s long in the case of ELENA at CERN. Furthermore the accuracy is of the order of 10^{-5} and the bandwidth of the order of hundreds of kHz (250 kHz in the PS).

For short measurements, it is possible to estimate the DC-offset voltage before starting the measurement and then subtract it from the data. However, in the case of long measurements, this correction is not suitable.

In three of the legacy B-train systems currently in operation at CERN, drift correction is made using special cycles, the so-called *zero cycles* or *zero pulse*, which are performed in some machines (PS, PSB, LEIR).

During these cycles there is no beam, so it is possible to short-circuit the input of the integrator and estimate the offset. Automatically the integrator subtracts the offset from the input voltage. Even if it is a very simple technique, this correction is partial because it considers only internal electronics, but the offset sources are in electronics, in the coil, in cables, thermoelectric voltages, noise and so on. Having a closed circuit input, the effect of the coil and cables as offset source will be lost. In addition, zero cycles are often available only sporadically, so the fluctuations of the offset cannot be followed very precisely. So this correction is not perfect and there is still a residual drift.

1.4 Motivation and objective of the thesis

For the requirements of our project, drift correction during long plateaux must have an accuracy of 10^{-5}. A correction at this level of accuracy, today it is impossible. In the coming years, the new B-train systems at CERN will have to face a number of metrological challenges including a higher accuracy, necessary to guide precisely ever more intense beams, and longer coil voltage integration times.

While in the old systems the integration is reset at every machine cycle i.e. every few seconds at most, the new B-trains will keep on integrating for weeks or even months without interruption. Of course, the existing dynamic field markers will keep providing a reference value at least once every cycle; however, new special cycles (see ELENA at Section 1.2.6) will include very long plateaux, during which dynamic marking is not possible. When we talk about a long plateau, we refer to the time interval during the cycle of a machine in which the magnetic field is ideally constant (Fig. 1.13). In order to carry out the correction we therefore need an instrument that can be interrogated. We will interrogate the instrument and it will give us, in the shortest possible time, the magnetic field value.

In this context, the main goals of this thesis are:

- mathematical modeling of the drift introduced by the integrator and a real-time correction mechanism of this offset;
- experimental characterization of the chosen NMR teslameter PT2026 as a DC-mode (static) field marker; in particular, estimation of the delay and jitter in communicating the measured field values;
- evaluation of the expected performance of the teslameter for integrator drift correction in the new B-train systems.

The main specifications of the systems are the following:

- typical uncertainty: a 10^{-5} relative to the peak field, i.e. 5 μT for ELENA;
- stability on long plateaux: 1 μT.

When we talk about long plateaux, we refer to the time interval during the cycle of a machine in which the magnetic field is constant.

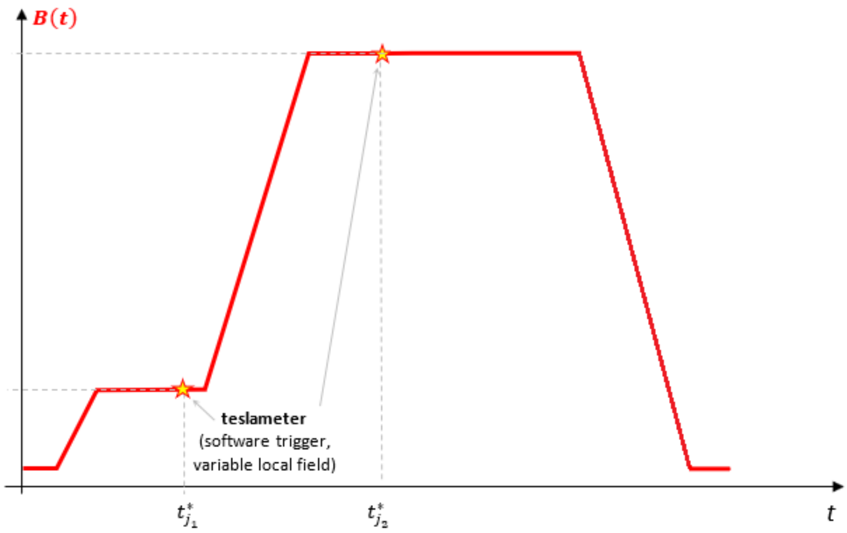

Figure 1.13: Magnetic field shape

Shape of a typical magnetic field cycle, including a flat-bottom (wait time between cycles at low level to minimize dissipation), and intermediate plateau (beam injection) and a flat-top (beam extraction). The beam is accelerated on the ramp-up and is not circulating on the ramp-down.

Chapter 2

Modeling and correction of integrator drift

2.1 Measurement model

The measurement model is based on segmenting the time axis into consecutive integration intervals, denoted by the index k, as shown in Fig. 2.3. For each interval, we start from the NMR value ($B^*(t^*{}_k)$), which is considered correct. We would like to have only $V_c(\tau)$ in the integration ideally, indeed the measured field can be expressed according to Equation 2.1:

$$B_m(t) = B^*(t^*{}_k) + \frac{1}{A_c}\int_{t^*{}_k}^{t} (V_c(\tau) + V_0(\tau))\, d\tau \qquad \text{for } t^*{}_k \leq t \leq t^*{}_{k+1} \tag{2.1}$$

where:

- A_c is the area of the coil;

- B^* is the integration constant, provided by the field marker;

- B_m is the measured field (with no drift correction);

- k is interval index;

- $t^*{}_k$ is the time of the field marker measurement;

- $V_0(t)$ is the voltage offset at the integrator's input;

- V_c is the voltage output of the coil ($V_c(\tau)=\frac{d\Phi}{dt}=A_c\frac{dB}{dt}$, where B is the average field over the coil and we ignore the minus sign of Lenz's law, via a suitable definition of the coil terminals).

Although this model is generally valid, we shall focus on finding a strategy to estimate and correct in real-time the drift on long cycle plateaux during which excitation current and field are approximately constant. In particular, we will consider a segmentation of the plateau in intervals of nominally equal length:

$$T^* = {t^*}_{k+1} - {t^*}_k \tag{2.2}$$

The actual magnetic field being given by:

$$B(t) = B^*({t^*}_k) + \frac{1}{A_c}\int_{{t^*}_k}^{t} V_c(\tau)\, d\tau \tag{2.3}$$

the measured field can be expressed as:

$$B_m(t) = B(t) + \frac{1}{A_c}\int_{{t^*}_k}^{t} V_0(\tau)\, d\tau \tag{2.4}$$

so that, substituting ${t^*}_{k+1}$ in (2.4), the accumulated measurement error during any integration interval is:

$$B_m({t^*}_{k+1}) - B({t^*}_{k+1}) = \frac{T^*}{A_c}\langle V_0\rangle \tag{2.5}$$

where the brackets $\langle . \rangle$ denote the mean value of the variable over the integration interval. The instantaneous field drift can be easily observed during a plateau, since:

$$\frac{dB}{dt} = 0 \quad \Rightarrow \quad \frac{dB_m}{dt} = \frac{V_0}{A_c} \tag{2.6}$$

Typically, V_c is between 100 mV and 5 V, while V_0 is up to hundreds of μV, so the relative error can be quite large. The uncertainty of the corrected field at the end of any integration interval can therefore be expressed as:

$$\sigma(B_m({t^*}_k)) = \frac{T^*}{A_c}\sqrt{\langle V_0^2\rangle} \tag{2.7}$$

where $\sqrt{\langle V_0^2\rangle}$ is the RMS average of the observed offset values. This uncertainty is reported in Table 5.1.

2.2 Experimental characterization of existing B-trains

Today, the B-train systems make a simplified real-time correction that does not use the field value provided by the field marker, but rather is based on short-circuiting the integrator input to estimate the voltage offset. Such correction is severely limited by the fact that it takes into account only a part of the offset sources, and also by its intermittent nature, constrained by operational considerations.

Typical values of the *field drift* come from an experimental estimate obtained and they are different for the various machines. In the Figure 2.1 and 2.2, the results of field drift measurements respectively for ELENA and PSB are shown. The values of the field drift are plotted as a function of the cycle index; in the case of ELENA a cycle lasted about 30 s, while in the case of the PSB it lasted about 1.2 s.

The voltage offset increment was calculated on field plateaux according to the Equation 2.14. The results are shown in the Table 2.1.

The measured values of voltage offset and drift are up to about a few dozen μV and up to 20 μT/s respectively. The voltage offset is clearly observed to fluctuate with respect to time; if it did not evolve over time, the estimate made in an interval would be the same in the next interval. The degree of variation over time can be expressed by the RMS of its time derivative, approximated by the discrete difference between consecutive cycles:

$$\sqrt{\left\langle \left(\frac{dV_0}{dt}\right)^2 \right\rangle} = \sqrt{\frac{1}{n_{cycles}-1}\sum_{i=2}^{n_{cycles}}\left(\frac{V_{0,i+1}-V_{0,i}}{\Delta t}\right)^2} \tag{2.8}$$

While in ELENA the offset tends to vary just by 10% over a total observation time of four minutes, the relative variation in PSB is much larger as the sign of the effect changes and the average is much smaller than the standard deviation. These differences in behavior are consistent with the experience of similar systems at CERN and may be ascribed to a number of factors, such as the length of the cabling between the sensors and the acquisition system, and the level of electrical noise in the environment.

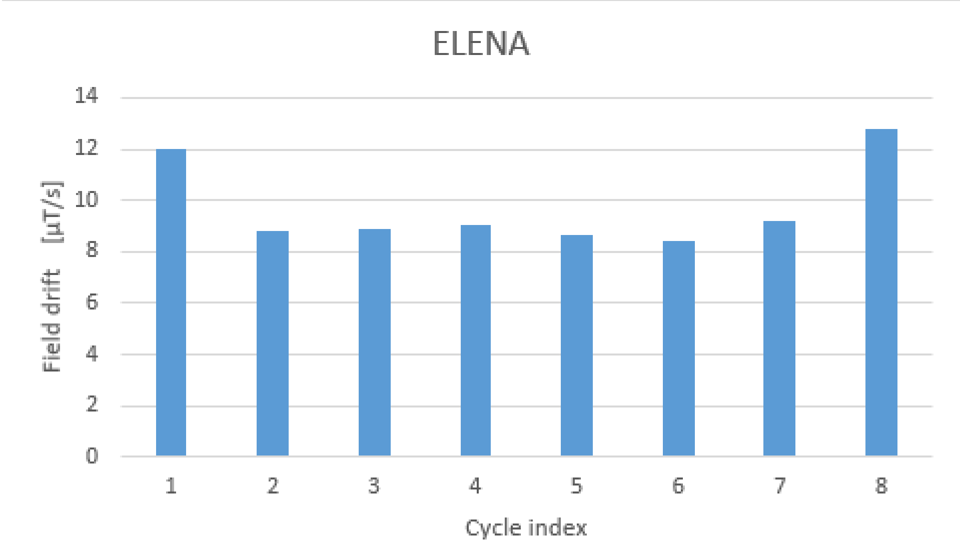

Figure 2.1: ELENA field drift measured over 30 s long cycles

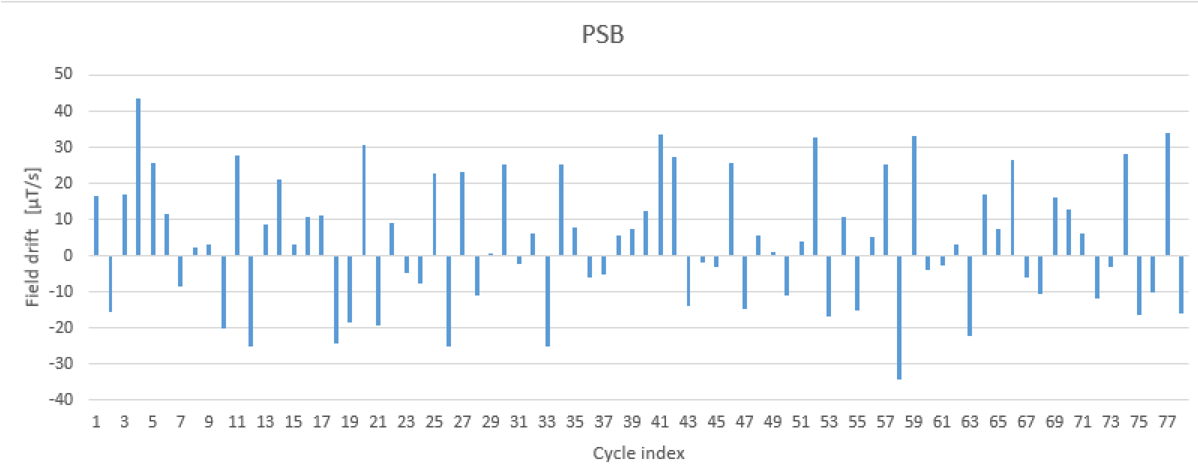

Figure 2.2: PSB field drift measured over 1.2 s long cycles

Machine	Coil Area [m²]	Voltage Offset			Field Drift (old correction)	
		Avg. [μV]	St. Dev. [μV]	RMS derivative [μV/s]	Avg. [μT/s]	St. Dev. [μT/s]
	A_c	$\langle V_0 \rangle$	$\sigma(V_0)$	$\sqrt{\langle \left(\frac{dV_0}{dt}\right)^2 \rangle}$	$\langle \frac{dB_m}{dt} \rangle$	$\sigma\left(\frac{dB_m}{dt}\right)$
ELENA	2.8	27.3	4.7	0.2	9.7	1.7
PSB	2.4	9.3	42.5	57.9	3.9	17.7

Table 2.1: Voltage offset and field drift observed in ELENA and PSB

2.3 Feed-forward drift correction

In the following sections a simplified analysis will be made to have an order of magnitude of the uncertainties involved.

The new feed-forward correction scheme is represented schematically in Fig. 2.3

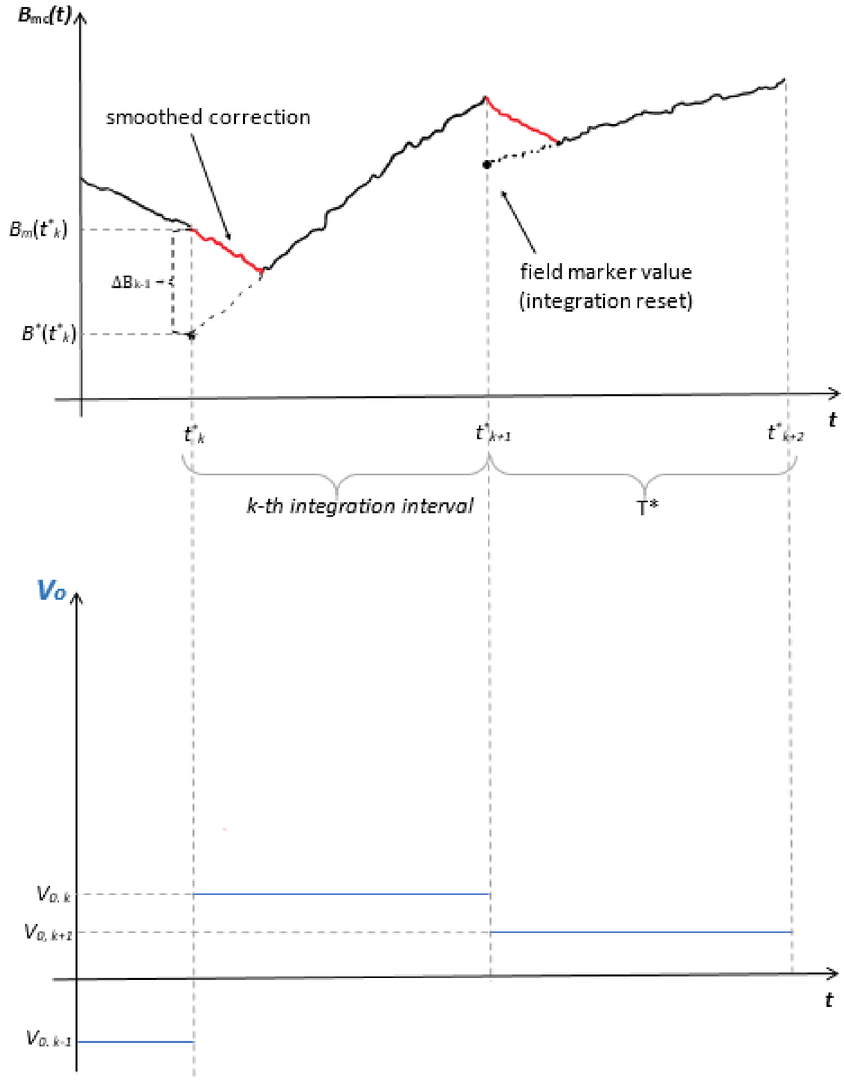

Figure 2.3: Measured corrected magnetic field and voltage offset

The working hypotheses are the following:

- quasi-static field throughout the measurement (we have already a method for correcting during ramps, i.e. dynamic field markers). The field is never truly constant due mainly to power supply ripple and drift, eddy currents and temperature effects;

- we assume constant drift in every interval.

During the k-th interval we shall represent the offset as the sum of two constants:

$$\widetilde{V}_{0,k} + \delta V_{0,k} = \frac{1}{T^*} \int_{t^*{}_k}^{t^*{}_{k+1}} V_0(\tau)\, d\tau \tag{2.9}$$

where $\widetilde{V}_{0,k}$ represents the average of the offset in the previous interval:

$$\widetilde{V}_{0,k} = \frac{1}{T^*} \int_{t^*{}_{k-1}}^{t^*{}_k} V_0(\tau)\, d\tau \tag{2.10}$$

and $\delta V_{0,k}$ is an unknown term that can be determined only at the end of the current interval, when a new marker measurement is available. Using these definitions, the measured field can be expressed as:

$$B_m(t) = B(t) + \frac{\widetilde{V}_{0,k}}{A_c}(t - t^*{}_k) + \frac{\delta V_{0,k}}{A_c}(t - t^*{}_k) \tag{2.11}$$

Since $\widetilde{V}_{0,k}$ is known during any given interval, we can use this knowledge to implement a real-time correction that, in a sense, feed-forward from the previous interval. The corrected field is defined by:

$$B_{mc}(t) = B_m(t) - \frac{\widetilde{V}_{0,k}}{A_c}(t - t^*{}_k) = B(t) + \frac{\delta V_{0,k}}{A_c}(t - t^*{}_k) \tag{2.12}$$

the field error ΔB_k at the end of the k-th interval is obtained from the NMR marker:

$$\Delta B_k = B_{mc}(t^*{}_{k+1}) - B^*(t^*{}_{k+1}) = \frac{\delta V_{0,k}}{A_c}\, T^* \tag{2.13}$$

It should be noted that this field correction is not to be applied instantaneously to the measurement but should rather be smoothed out, as indicated by the red segments in Fig. 2.3, in order to avoid discontinuities that can impact negatively the users of the B-train.

From Equation 2.13 the offset increment is calculated as:

$$\delta V_{0,k} = \frac{A_c}{T^*}\, \Delta B_k \tag{2.14}$$

Knowledge of the increment will be then incorporated in the constant to be used during the next interval:

$$\widetilde{V}_{0,k+1} = \widetilde{V}_{0,k} + \delta V_{0,k} \tag{2.15}$$

The relationship between the offset in the two consecutive intervals can be expressed as:

$$\widetilde{V}_{0,k+1} + \delta V_{0,k+1} = \widetilde{V}_{0,k} + \delta V_{0,k} + \sqrt{\left\langle \left(\frac{dV_0}{dt} \right)^2 \right\rangle} T^* \tag{2.16}$$

where the average time derivative can be obtained from the discrete approximation seen above (Table 2.1). By substituting Equation 2.15 we see that:

$$\delta V_{0,k+1} = \sqrt{\left\langle \left(\frac{dV_0}{dt} \right)^2 \right\rangle} T^* \tag{2.17}$$

which shows, as intuitively expected, that the offset increment represents the component that fluctuates randomly over time.

Finally, note that correction of the distributed field is already applied in the existing B-trains: what is missing is the iterative estimation and subtraction of the offset.

2.4 Uncertainty analysis

The standard uncertainty associated to the various steps of the correction procedure are discussed in this section. So we shall attempt to make an estimation of the errors inherent in this analysis.

First, the uncertainty of the offset increment can be estimated by error propagation in Equation 2.14, obtaining:

$$\frac{\sigma^2(\delta V_0)}{\delta V_0^2} = \frac{\sigma^2(A_c)}{A_c^2} + \frac{\sigma^2(T^*)}{T^{*2}} + \frac{\sigma^2(\Delta B)}{\Delta B^2} \tag{2.18}$$

In this expression we find three contributions:

- the relative uncertainty of the coil surface area, which is typically 10^{-4};

- the relative uncertainty of the field difference. The NMR measurement (B^*) is in the range of a few 10^{-6} and therefore does not practically contribute to the uncertainty, while the measurement derived from the flux integrator is also of order 10^{-4};

- the relative uncertainty of the time interval duration, which is the object of the present work. As it will be shown in Chapter 4, this term can reach up in the percent range and is therefore largely dominant.

As a result Equation 2.18 can be simplified to Equation 2.19:

$$\frac{\sigma^2(\delta V_0)}{\delta V_0^2} \approx \frac{\sigma^2(T^*)}{T^{*2}} \Rightarrow \frac{\sigma(\delta V_0)}{\delta V_0} \approx \sqrt{2}\,\frac{\sigma(t^*)}{T^*} \tag{2.19}$$

where we have obtained from (2.2):

$$\sigma(T^*) \approx \sqrt{2}\,\sigma(t^*) \tag{2.20}$$

and $\sigma(t^*)$ represents the uncertainty of each time measurement, which is determined experimentally in Chapter 4.

From the expression above, we see that timing errors are the major source leading to an error in the estimation of the current offset, which of course causes an error in the field measured during the next interval. Another source of error is the time fluctuation of the offset, which can be predicted only statistically. As a result, by error propagation in (2.16) we find that the total uncertainty of the voltage offset during the next interval is:

$$\sigma^2(\widetilde{V}_{0,k+1} + \delta V_{0,k+1}) = \sigma^2(\delta V_{0,k}) + \left\langle \left(\frac{dV_0}{dt}\right)^2 \right\rangle \sigma^2(T^*) \tag{2.21}$$

The uncertainty of the offset increment can be obtained from (2.19):

$$\sigma^2(\delta V_{0,k}) = 2\,\frac{\sigma^2(t^*)}{T^{*2}}\,\langle \delta V_{0,k}^2 \rangle \tag{2.22}$$

where we took the RMS of the increment to represent its typical value. This, in turn, can be computed from the experimental data in (Table 2.1) using (2.17):

$$\langle \delta V_{0,k}^2 \rangle = \left\langle \left(\frac{dV_0}{dt}\right)^2 \right\rangle T^{*2} \tag{2.23}$$

For any voltage offset with a given uncertainty, the uncertainty of the measured field can be expected to grow linearly from zero at the time ${t^*}_{k+1}$ of marker rest to a maximum value at the end of the next interval, which is proportional to the interval duration and to the offset uncertainty:

$$\sigma(B_{mc}({t^*}_{k+2})) = \frac{T^*}{A_c}\sqrt{\left\langle \left(\frac{dV_0}{dt}\right)^2 \right\rangle (2\sigma^2(t^*) + \sigma^2(T^*))} = 2\,\sigma(t^*)\,\frac{T^*}{A_c}\sqrt{\left\langle \left(\frac{dV_0}{dt}\right)^2 \right\rangle} \tag{2.24}$$

This expression shows how the two field error sources combine and is plotted in Fig. 5.1 for the two experimental cases of ELENA and PSB.

Chapter 3

NMR PT2026

The teslameter PT2026 is a magnetometer, i.e. an instrument that measures magnetic flux density. The measuring technique is the Nuclear Magnetic Resonance (NMR), which guarantees extreme precision and accuracy and for this reason it is useful to calibrate other magnetometers. In addition, the NMR magnetometers are also used in many scientific and industrial applications, where there is a need to monitor or adjust magnetic fields with extreme precision.

Figure 3.1: Metrolab PT2026 NMR teslameter

3.1 Measurement

The main improvements of the teslameter PT2026 compared to the previous model (PT2025) are the following:

- Pulsed-wave: the sample is excited with a short pulse. The teslameter PT2026 supports both continuous-wave and pulsed-wave, while the old teslameter only supports continuous-wave. For this reason, the teslameter PT2025 takes much longer to find resonance; in the worst case of the experience at CERN, locking can take up to the order of 1 minute. This new mode guarantees a fast measurement rate: this is the strong point of PT2026. It allows measurement rates up to 33 Hz, instead of the PT2025's 1 Hz;
- metrological standard: it is a metrological standard because it is not possible to measure magnetic fields in a more precise way. In fact it has an accuracy of the order of ppm. Despite the high cost, it is used as often as possible.

However, besides the advantages, there are also some disadvantages for the NMR magnetometry:

- NMR is best suited for measuring strong magnetic fields ($\geq$ 40 mT [14]) (the so-called flowing water techniques has been developed for lower fields, but this is rather complex and unpractical);
- it only works well in a uniform magnetic field. If the field is not uniform, the measurement takes longer and becomes less precise because the resonance spreads out;
- NMR is a relatively slow measurement technique (33 Hz in the best case).

The new teslameter allows to make measurements triggered both continuously, at regular intervals, and through a TTL signal and it can generate an output trigger when a certain field value has been reached.

There are three standard PT2026 probes that differ in range and, thanks to the LabVIEW Instrument Driver, it is possible to easily write control programs for the teslameter.

3.2 Interfaces

As regards the interfaces, the teslameter PT2026 is compliant to some of the most important industry standards.

It supports two physical host interfaces:

1. USB 2.0: the teslameter allows an USB full-speed communication (12 Mbps) and it is possible to connect it with any USB-capable computer;
2. Ethernet: this interface can reaches 10 Mbps or 100 Mbps, in Full or Half Duplex mode.

Furthermore, it supports two host interface protocols:

1. *native*: this protocol is based on the following standards:
   - IEEE 488.2: for the device control. Thanks to this protocol, any VISA library can control every aspect of the instrument;
   - USBTMC-USB488: for USB device control. In this way, the instrument can be connected without needing a custom usb driver;
   - VXI-11: for Ethernet device control. It provides the same advantages as USBTMC for USB;
   - SCPI: in order to define a command structure and provide a programming interface familiar to several instrumentation system programmers. *The Standard Commands for Programmable Instruments* (**SCPI**) was used instead to send *set* or *query* operation to the device. It is a standard that provides commands and syntax to use in controlling measurement devices. The commands are ASCII textual strings and they are sent to the device over the physical layer. They are composed of a set of keywords and queries end with a question mark so that some commands can be used for both performing a query operation or a set operation.

     The command syntax uses a *tree* structure in order to group similar commands [24]. Sub-commands follow the previous command within the hierarchy with a colon character. For example there are a lot of information concerning the probe connected to the given channel; so if we are interested in the model of the probe, we will use *:ROUTe:PROBe:MODel?*, on the contrary if we are interested in the serial number of the probe, we will use *:ROUTe:PROBe:SERialno?*.

The commands for the set operation require an additional argument that are separated by a space from the previous command. For example, in order to set the format of the data as ASCII, we will use the command *:FORMat:DATA ASCii*.

Finally, it is possible to use the abbreviated form for the commands only sending the characters in the upper case; for example, *:FORMat* has the same effect of *:FORM*.

2. *MODBUS*: PT2026 supports this protocol only on the Ethernet interface and, typically, it is a protocol used in industrial automation applications.

3.3 Instrument performance stand-alone

The table of specifications, taken from the teslameter manual [14], is the following

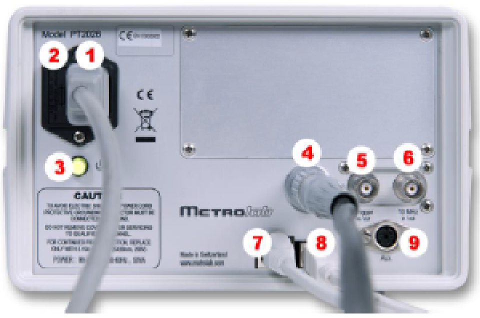

1	Power	50 W, 90 – 260 VAC, 50/60 Hz
2	Fuse	3.15 A (T), 5x20 mm, 250 V
3	Power switch	The front- and back-panel switches have the same functions: • Power on: with power off, hold ~1 sec • Power off: with power on, press momentarily • Factory reset: with power on, hold until power-off (~5 sec) • Forced shutdown: when system is hung, hold until power-off (~10 sec)
4	Probe	The same connector is used for multiplexers and other PT2026 accessories; proprietary pin-out.
5	Trigger	TTL Level; trigger output or input: • Trigger output: flags when field attains a given value; B rising, falling or either; pulse or level output; can drive 50Ω. • Trigger input: determines when measurement is taken; rising or falling edge; high impedance input.
6	Reference clock	• Internal reference output: 10 MHz ± 1 Hz, can drive 50Ω. • External reference input: 10 MHz ± 30 Hz, 50Ω input.
7	Ethernet	RJ45
8	USB	USB 2.0, Standard B connector
9	Auxiliary 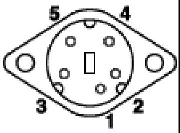	Mini DIN 5: 1. On/Off: short to ground is like pressing power switch; 2. NMR signal output; 3. Modulation output (continuous-wave only); 4. Sync output (pulsed-wave only); 5. Ground.

Table 3.1: Back Panel

MEASUREMENT

Frequency range	1 MHz – 1 GHz
Resolution	± 0.1 Hz (stable field, low gradient, no averaging)
Accuracy	± 5 ppm, independent of temperature
Max gradient	> 1000 ppm/cm
Measurement rate	Up to 33 Hz
Trigger modes	Immediate, Timed, Bus, External

Table 3.2: Measurement

PROBES

Ranges	0.19 – 0.52 T (4 mm Ø p sample) 0.42 – 1.29 T (3 mm Ø p sample) 1.13 – 3.52 T (3 mm Ø p sample) 3.29 – 10.57 T (3 mm Ø p sample) 8.00 – 22.8 T (3 mm Ø D sample) Custom ranges upon request
Size	Standard probe / electronics: 16 x 12 x 231 mm Remote measurement head: 11. Head (p sample): 9.2 x 6.2 x 31.5 mm 12. Head (D sample): 16.2 x 6.2 x 31.5 mm
Cable length	10 m; custom upon request 100 m max total length (incl. multiplexers) Remote measurement head: 13. Electronics – head: 3 m (Ø 4.3 mm)
Search time	Full range typ. < 10 s
Multiplexer (optional)	Self-powered; 4 or 8 channels; up to 3 levels (512 probes max)

Table 3.3: Probes

Chapter 4

Testing acquisition times and readout delay

4.1 Test setup and configuration

In order to use the teslameter for the following tests, an Ethernet connection was used between the PC and the teslameter. Ethernet was chosen because the module created during my work will be integrated into a framework where there are already some modules that use Ethernet for communication.

For the measurement of the magnetic field we chose to use the continuous mode of operation because we want to have the flexibility and efficiency to request the measurement in an adaptive way, that is, we want to use the device by making a request via software, when we have need to correct. In particular, the steps taken are as follows:

1. ask the instrument to make the measurement;
2. wait for the measure;
3. read the answer.

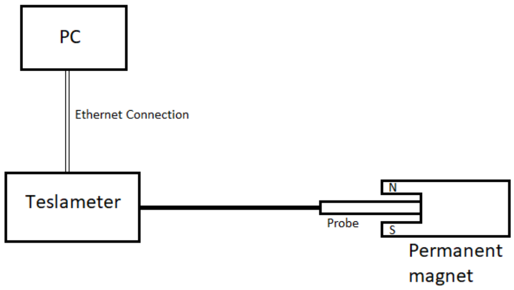

Figure 4.1: Test setup block diagram

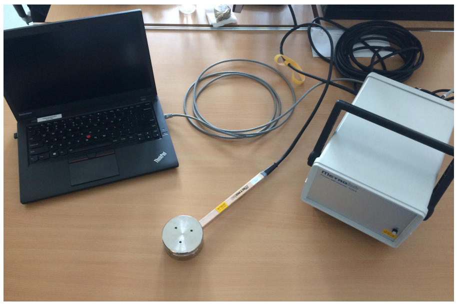

Figure 4.2: Test setup

The PC has CentOS [25] as operating system and a C program was used to communicate with the instrument. Metrolab's software allows to display the results both numerically and in form of graphs, but it was only made for Windows.

The version 17.0 of NI-VISA was downloaded, where NI-VISA is the National Instrument implementation of VISA I/O standard, including software libraries and configuration program. The Virtual Instrument Software Architecture (VISA) is *"a standard for configuring, programming, and troubleshooting instrumentation systems comprising GPIB, VXI, PXI, Serial, Ethernet, and/or USBinterfaces"* [26].

The tests have been done with the teslameter PT2026, a NMR permanent magnet and a Metrolab standard probe that have the following features:

Magnet type	PM-1055-050N
Magnet field	0.290T @ 24°C
Magnet T.C.	-1200 ppm/°C
Probe Model	1226
Probe Range	0.19-0.52 [T]
Teslameter Model	PT2026
Teslameter S/N	00037
Teslameter accuracy	±5 ppm, independent of temperature
Teslameter measurement rate	up to 33 Hz

Table 4.1: Features of NMR permanent magnet, probe and teslameter

4.2 Communication and interaction

The main VISA functions used in the C program for the communication and the acquisition of the field values are the following:

- **viOpenDefaultRM()**: it allows to create a communication channel with the VISA driver. It returns *VI SUCCESS* if a session is created successfully;
- **viOpen()**: it creates a communication channel to the device. It uses the variable returned from *viOpenDefaultRM()* and returns *VI SUCCESS* if a session is opened successfully;
- **viSetAttribute()**: it is used to set the time-out during the communication with the device associated with a certain session. In this case it has been set to 5000 ms.
- **viWrite()**: it allows to write data to the device. It returns *VI SUCCESS* if the transfer has been completed successfully.
- **viRead()**: it reads data from the device. It returns *VI SUCCESS* if the operation has been completed successfully.

- **viClose()**: it closes the specified session. *VI SUCCESS* indicates that the session was closed correctly.

The SCPI command used in the C program are the following:

- ***IDN?**: it returns information regarding the teslameter such as the manufacturer, the model, the serial number, etc.

Listing 4.1: IDN query command

```
void idn(ViSession instr, ViSession resource_manager, ViUInt32 io_byt,
ViStatus status){

        const ViUInt32 Bsize = 1000;
        ViChar buffer[1000];

        ViBuf scpi_command = "*IDN?";
        status = viWrite(instr, scpi_command, (ViUInt32)strlen(scpi_command),
        &io_byt);
        if (status < VI_SUCCESS) {
                printf("Error writing to instrument\n");
                viStatusDesc(resource_manager, status, buffer);
                printf("%s\n", buffer);
                return 0;
        }
// Read response from instrument
        status = viRead(instr, buffer, Bsize, &io_byt);
        if (status < VI_SUCCESS) {
                printf("Error reading from instrument\n");
                viStatusDesc(resource_manager, status, buffer);
                printf("%s\n", buffer);
                return 0;
        }
    ...

}
```

- **:FORM ASC**: it sets the format for returned data as ASCII

Listing 4.2: Set format command

```
void set_ascii (ViSession instr, ViSession resource_manager, ViUInt32 io_byt,
ViStatus status){

        ViChar buffer[1000];

        ViBuf scpi_command = ":FORM ASC";
        status = viWrite(instr, scpi_command, (ViUInt32)strlen(scpi_command),
        &io_byt);
        ...
}
```

- **:ROUT:PROB:SCAN?**: it returns an array of all channels with a probe connected

Listing 4.3: Scan query command

```
void scan(ViSession instr, ViSession resource_manager, ViUInt32 io_byt,
ViStatus status){
        ...
        ViBuf scpi_command = ":ROUT:PROB:SCAN?";
        status = viWrite(instr, scpi_command, (ViUInt32)strlen(scpi_command),
        &io_byt);
        ...
        // Read response from instrument
        status = viRead(instr, buffer, Bsize, &io_byt);
        ...
}
```

- **:ROUT:CLOS (@1)**: it allows to select the first channel

Listing 4.4: Channel selection command

```
void select_channel(ViSession instr, ViSession resource_manager,
ViUInt32 io_byt, ViStatus status){
```

```
    ...
    ViBuf scpi_command = ":ROUT:CLOS (@1)";
    status = viWrite(instr, scpi_command, (ViUInt32)strlen(scpi_command),
    &io_byt);
    ...
}
```

- **:INIT:CONT 1**: it puts the instrument in continuous acquisition mode. This means that it will measure at its fastest rate

Listing 4.5: Init command

```
void start_meas(ViSession instr, ViSession resource_manager, ViUInt32 io_byt,
ViStatus status){
    ...
    ViBuf scpi_command = ":INIT:CONT 1";
    status = viWrite(instr, scpi_command, (ViUInt32)strlen(scpi_command),
    &io_byt);
    ...
}
```

- **:STAT:OPER?**: it allows access to the *Operation Status Register*

Listing 4.6: Status Operation query command

```
ViChar *stat(ViSession instr, ViSession resource_manager, ViUInt32 io_byt,
ViStatus status){
    ...
    ViBuf scpi_command = ":STAT:OPER?";
    status = viWrite(instr, scpi_command, (ViUInt32)strlen(scpi_command),
    &io_byt);
    ...
    // Read response from instrument
    status = viRead(instr, buffer, Bsize, &io_byt);
     ...
  }
```

- **:FETC:SCAL:FLUX?**: it fetches the values acquired during last INIT. This operation clears the New Measurement Available bit

Listing 4.7: Fetch command

```
ViChar *fetch_flux(ViSession instr, ViSession resource_manager,
ViUInt32 io_byt, ViStatus status){
        ...
        ViBuf scpi_command = ":FETC:SCAL:FLUX?";
        status = viWrite(instr, scpi_command, (ViUInt32)strlen(scpi_command),
        &io_byt);
        ...
        // Read response from instrument
        status = viRead(instr, buffer, Bsize, &io_byt);
        ...
}
```

The functions were called following the same order as the previous list and a particular attention has been given to the status operation command.

The *Operation Status Register* was added by the SCPI standard to the two registers contained by all IEEE 488.2 compliant instruments (*Status Byte* and *Standard Event Status Register*). The table below, taken from PT2026 User Manual [14], describes how the teslameter uses the *Operation Status Register*.

Bit	Name	Description
2	RANGing	Scanning for available probes
3	SWEeping	Searching for NMR signal
4	MEASuring	Measuring magnetic field strength
5	Waiting for TRIGger	Waiting for trigger
8	New Acq Avail	New Acquisition Data is Available
9	New Meas Avail	New Measurement Available
11	BIT11	Summary Bit: A parameter has changed
12	BIT12	Summary Bit: Acquisition status

Table 4.2: OPERation Status Register

The bit to check, in order to determine if there is a new measurement available is the bit 9 of the *Operation Status Register*. So, after starting the measurement in continuous mode it is necessary to poll the *New Measurement Available* bit. Only when this bit is set, it is possible to collect the data with the command *:FETC:SCAL:FLUX?*. In order to determine the value of the 9th bit of the result of the *:STAT:OPER?* command, we need to mask it

Listing 4.8: Polling on the New Measurement Available

```
    ...
    do{
        stat_op=stat(instrument, resource_manager,io_bytes, status);
        stat_op_int=atoi(stat_op);
        i++;
    }while((stat_op_int & 0x200) == 0);
    ...
fetch_value=fetch_flux(instrument, resource_manager, io_bytes, status);
```

4.3 Timing performance

For logistical reasons it was not possible to find a measuring laboratory for experimental tests and for this reason they were performed in my office. Three timestamps were taken using the function *gettimeofday()*:

- a timestamp before the measurement (t_{in}), when the request is first made;
- a timestamp after the measurement (t_1);
- a timestamp after the transmission (t_2).

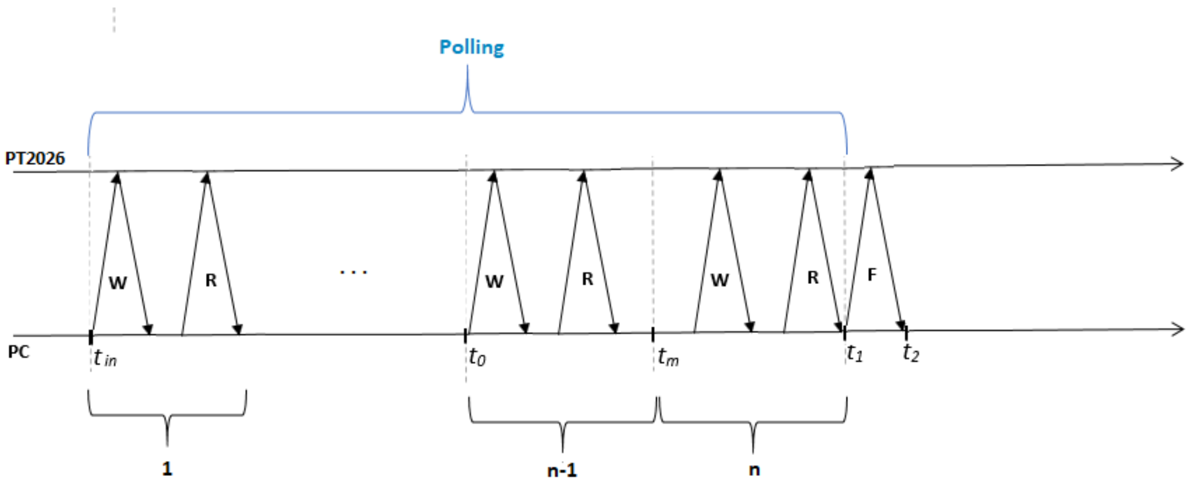

Figure 4.3: Communication diagram

where the symbols W, R and F respectively indicate write, read and fetch operation.

The iteration 1 represents the first request made to the teslameter, which will initially have a negative result. After a number n of iterations, which in the test has been on average 5, the New Measurement Available bit will be set and the fetch phase will be performed to read the value. Moreover, the average duration of a cycle, consisting of a write and a read, is about 7 ms.

The instant of time in which the measure took place is between the instant t_0 and t_1. In order to minimize the maximum error we consider it at the center of the interval $[t_0,t_1]$

$$t_m = \frac{t_1 - t_0}{2} \pm \underbrace{\frac{t_1 - t_0}{2}}_{uncertainty} \tag{4.1}$$

Thanks to these timestamp values, an evaluation was possible both for the measurement times and for the readout delay. The overhead in addition to the measurement and transmission phases is less than 10 μs, so it is negligible compared to the rest, so it is possible to assume that the difference between t_m and t_{in} represents the time needed for the measurement, while the difference between t_2 and t_m represents the delay for the transmission.

4.3.1 First Test

The first test was made with a set of 10000 consecutive measurements. It was performed during the morning and lasted about 10 minutes.

Field values analysis

The following graph shows the raw field as a function of the time

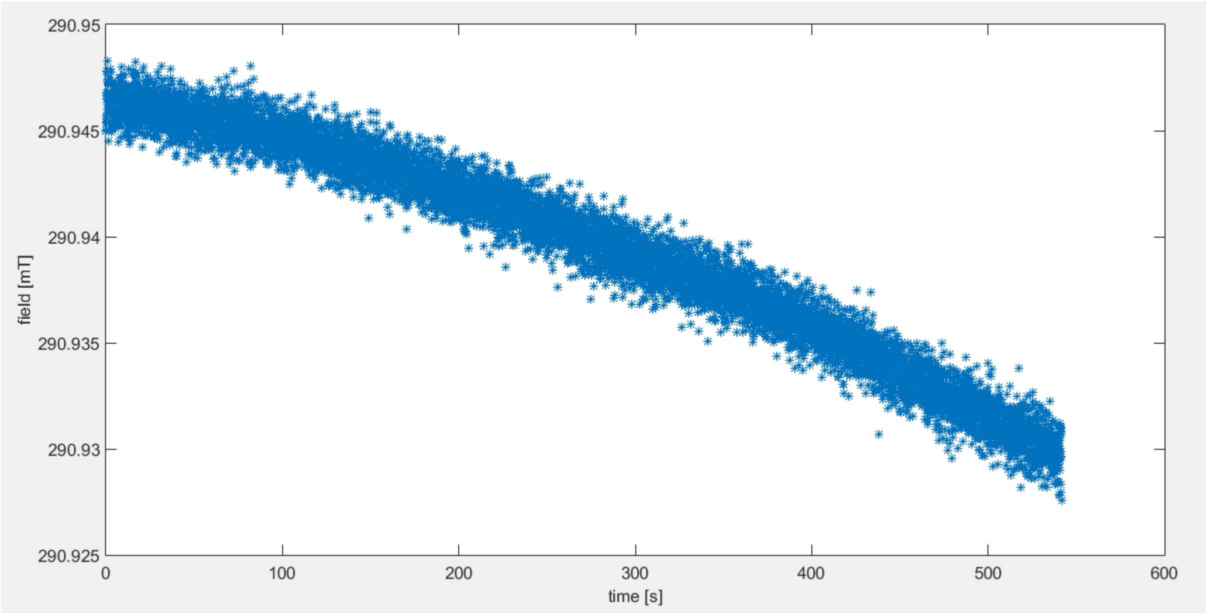

Figure 4.4: Raw field values

The graph shows a trend due to a thermal effect, in particular it depends on the temperature of the environment and of the probe. In fact, the relative drift is given by

$$\frac{\text{max value} - \text{min value}}{\text{mean value}} = 68.74 \text{ ppm} \tag{4.2}$$

Considering that from the specifications of the permanent magnet (4.1) the temperature coefficient is -1200 ppm/°C, the corresponding temperature increase is

$$\frac{68.74}{1200} = 0.0573\ ^{\circ}C \tag{4.3}$$

which is compatible with ambient conditions. In this test, the measurements were made during the morning and the temperature increase is shown by the decreasing trend of the field (Figure 4.4).

Since the variation due to temperature is not of our interest, the drift is was subtracted from the measured field values, through a moving average.

So, the normalized measurement is represented in the following figure

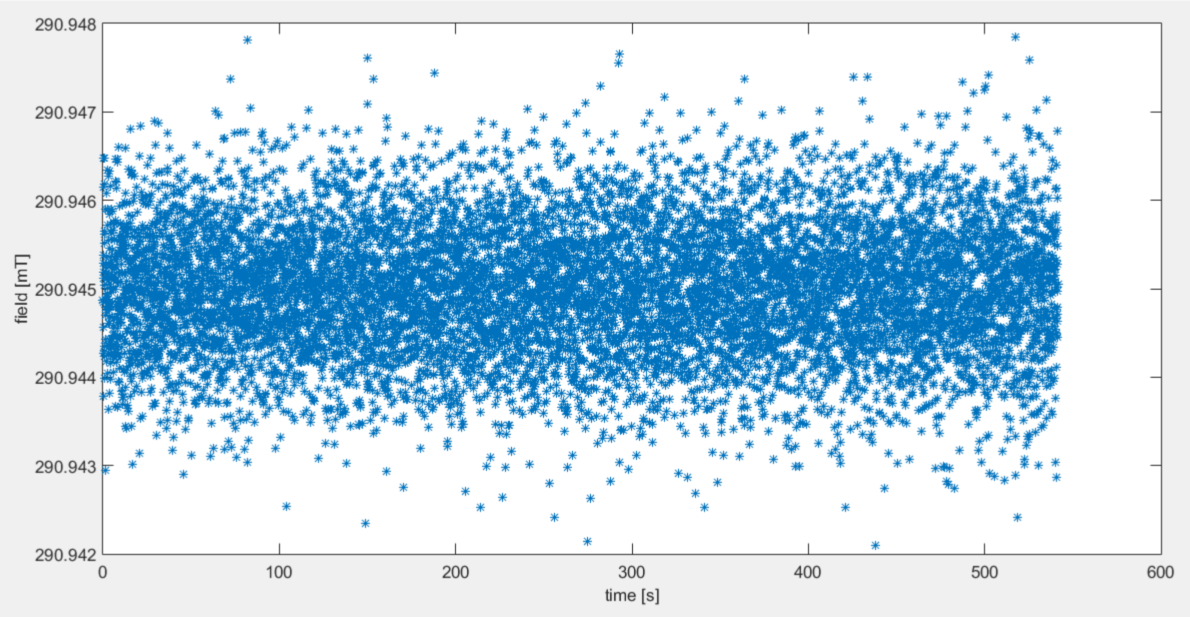

Figure 4.5: Normalized field values

The histogram of the field values is the following

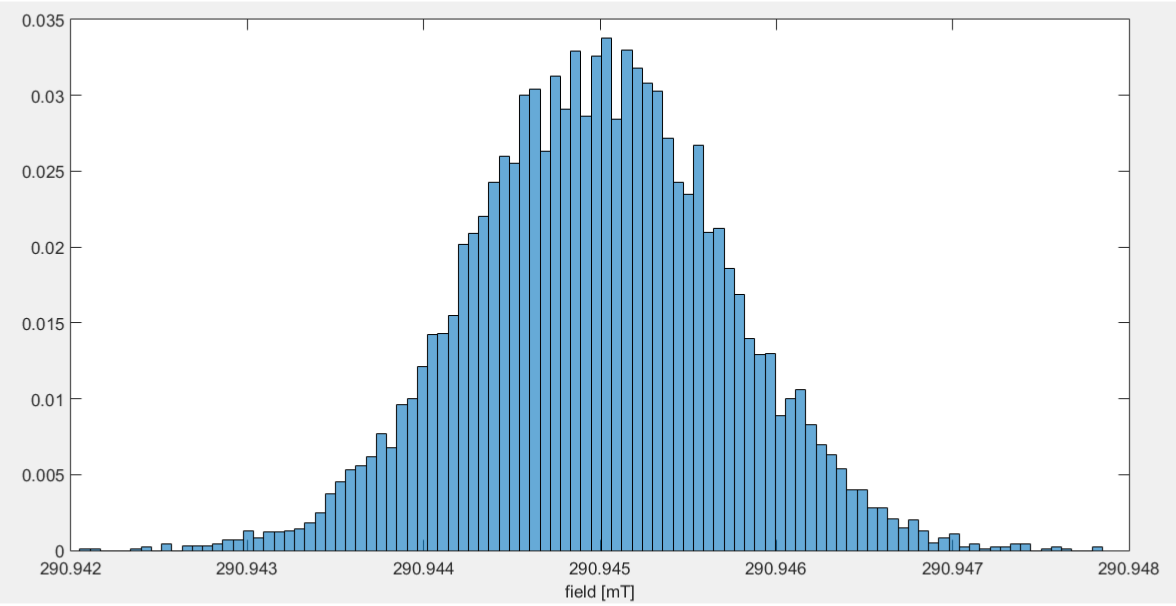

Figure 4.6: Field value histogram

The statistics of the field values are shown in Table 4.3

Parameter	Value [mT]
Mean	290.944
Standard Deviation	7.229×10^{-4}
Min	290.942
Max	290.947
Mode	290.944

Table 4.3: Field parameters

Observations:

- random nature of the noise confirmed by the Gaussian shape (Figure 4.6);
- with reference to the table 4.3, the dispersion of the field values in relative terms is

$$\frac{\text{Standard Deviation}}{\text{Mean}} = \frac{0.723\ \mu\text{T}}{290944\ \mu\text{T}} = 2.48 \cdot 10^{-6} \approx 3\ \text{ppm} \tag{4.4}$$

  this is compatible with the specification of the instrument (±5 ppm [14]);
- the mean field value is compatible with the nominal field of the magnet (Table 4.1), at a temperature of about 26 degrees, which is compatible with the ambient conditions.

Timing analysis

A first iteration of the measurement, shown in Figure 4.8, was made with the probe simply inserted in the magnet.

Figure 4.7: Probe not fixed

In this case, the measurement duration reaches up to 300 ms, which is grossly inconsistent with the specification (up to 33 Hz [14]). In fact, on average, the teslameter will take more time to perform the measurement.

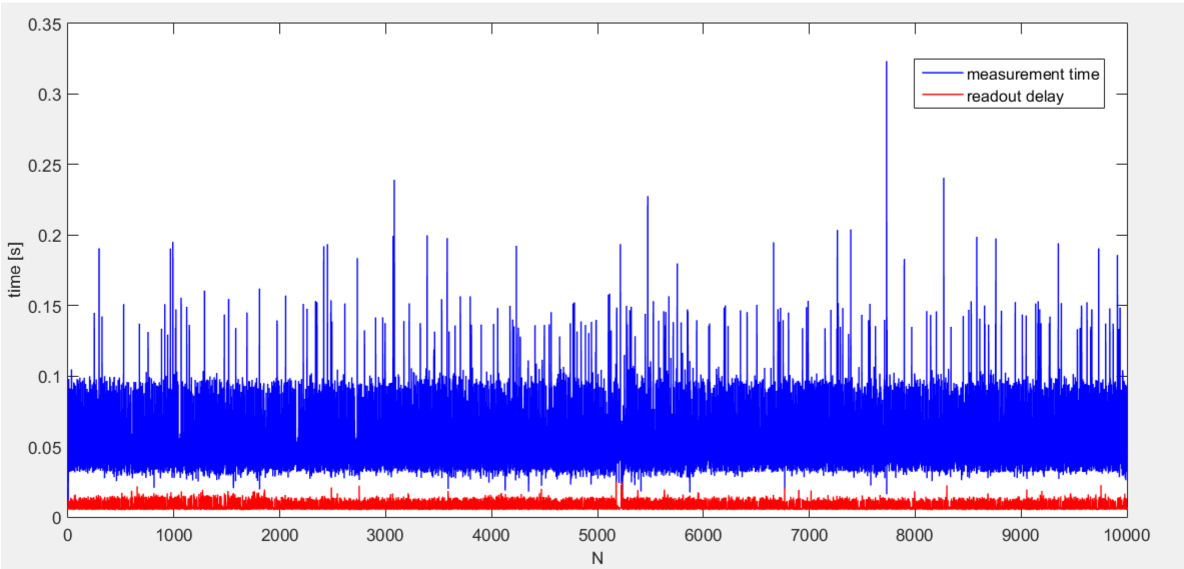

Figure 4.8: Measurement time and readout delay

After a series of attempts I understood that the problem was the unstable position of the probe, so the probe was placed under better mechanically controlled conditions

Figure 4.9: Probe fixed

In this way, the results were the following

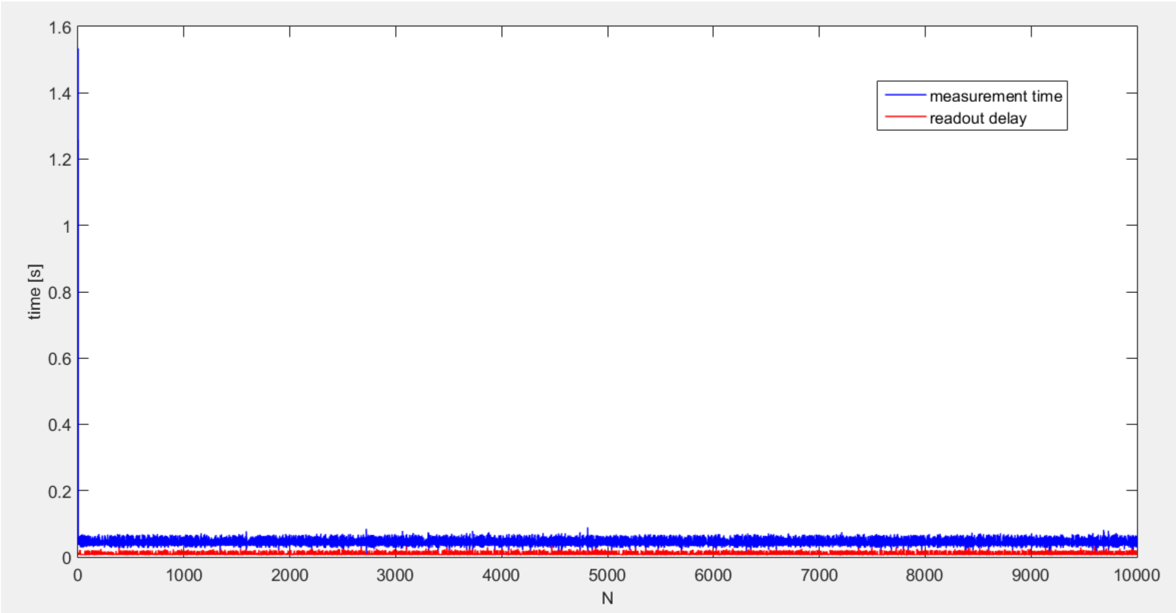

Figure 4.10: Measurement time and readout delay

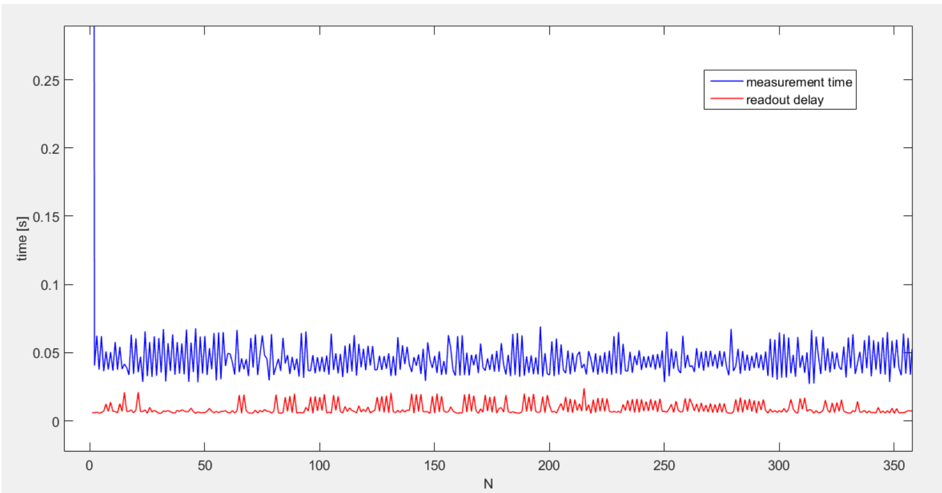

Figure 4.11: Zoom of the previous graph

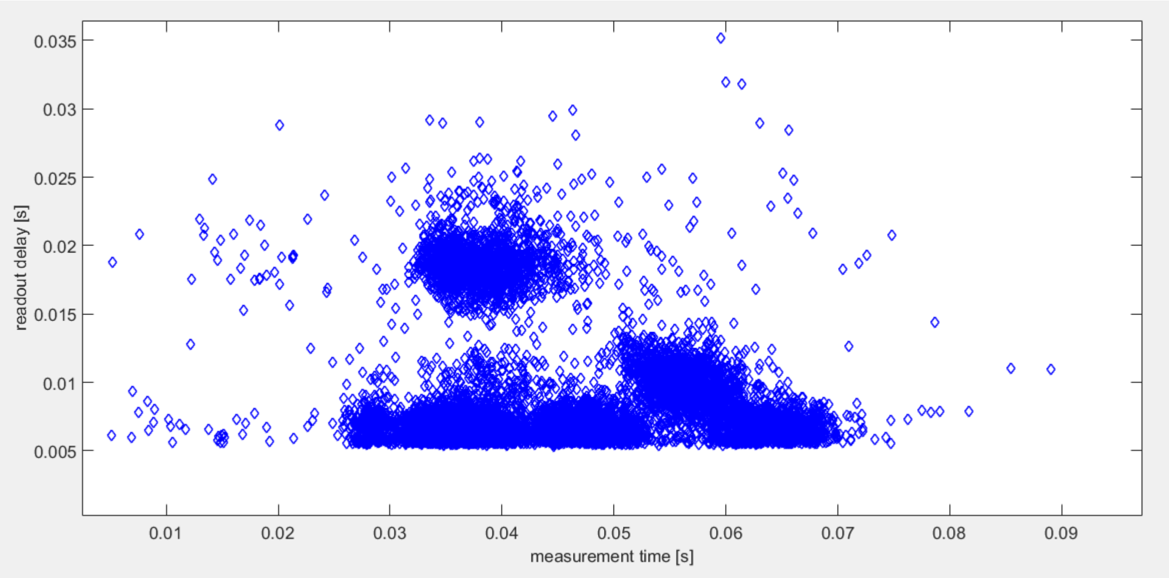

Figure 4.12: Dispersion graph

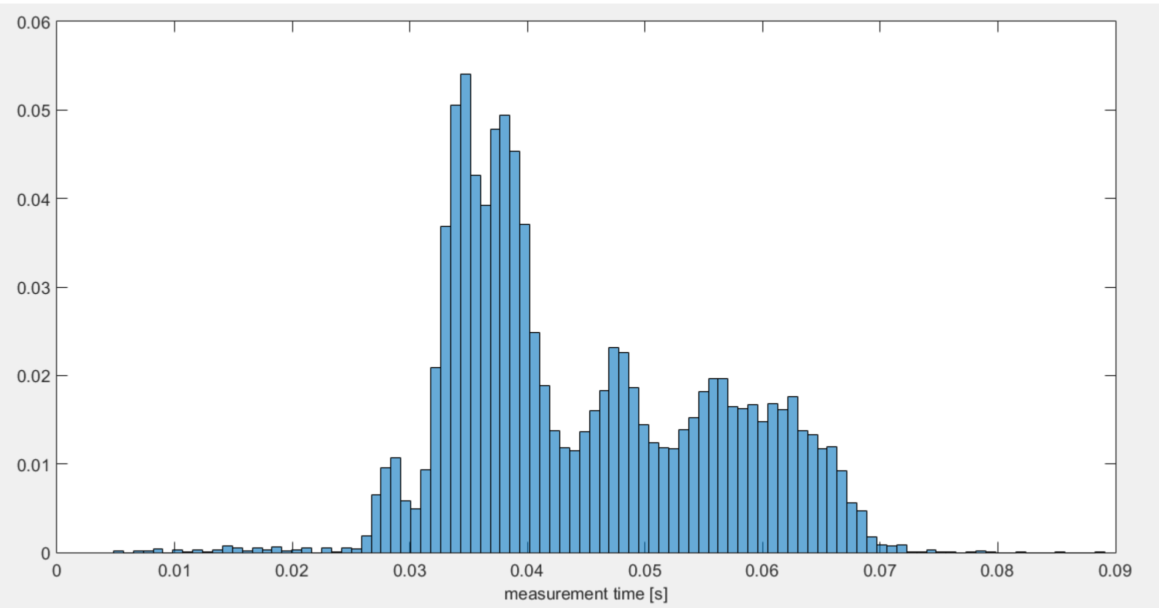

Figure 4.13: Measurement time histogram

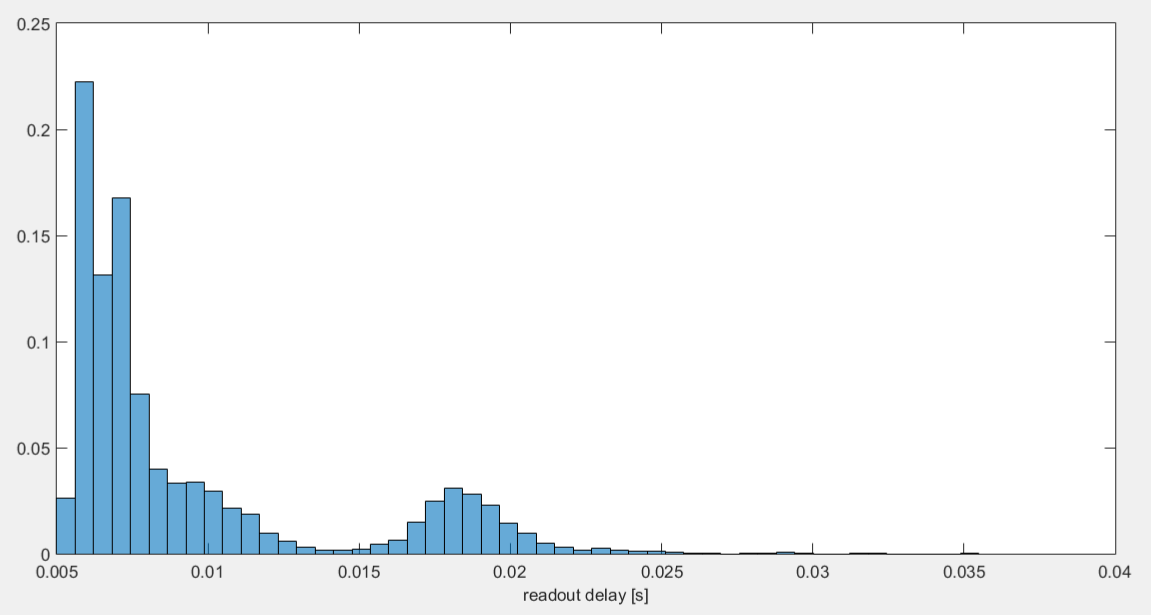

Figure 4.14: Readout delay histogram

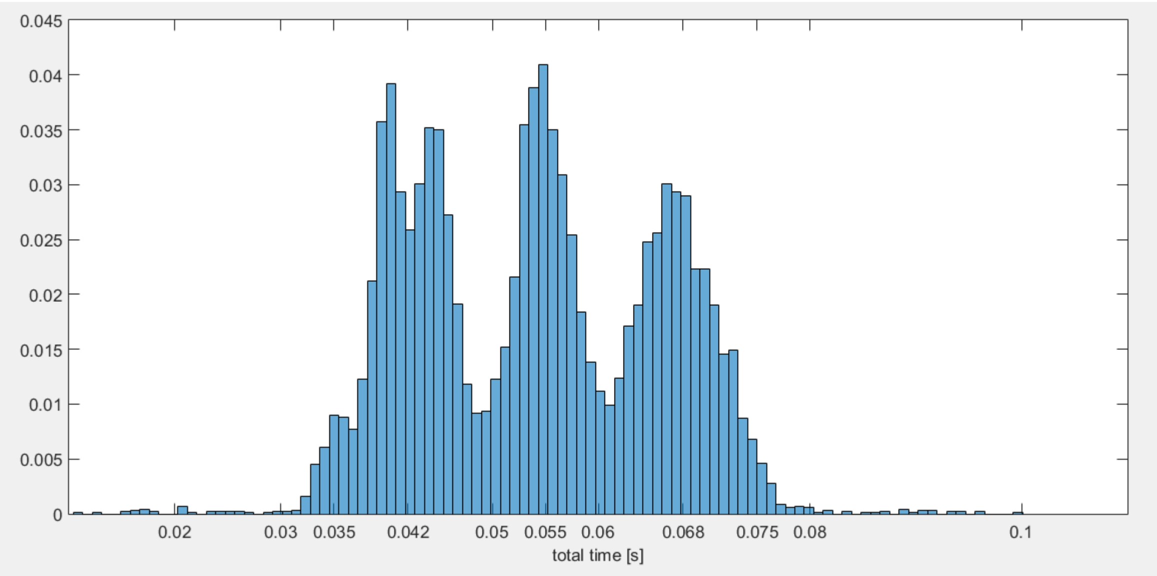

Figure 4.15: Total time histogram

The results of the statistical analysis of measurement time and readout delay are shown in Table 4.4

Parameter	Measurement time [ms]	Readout delay [ms]	Total time [ms]
Mean	44.899	9.41	54.31
RMS	48.618	10.53	57.468
Standard Deviation	18.647	4.723	18.786
Min	5.08	5.31	11.183
Max	89.056 (1534.08)	35.187	100 (1540.077)
Mode	34.399	6.916	45.351

Table 4.4: Time parameters

Observations:

- in Figure 4.10 it is possible to observe that the maximum value is the first value of the measurement time; this is due to the time needed by the probe to acquire the NMR signal. Once the NMR signal has been found, the instrument will start measuring and the time required to the transmission, on average, is less than the time for measurement (neglecting the initial value, the maximum value for the transmission time is 89.056 ms);
- in order to verify if there is a relationship between the two parameters (measurement and transmission time), a correlation coefficient was calculated:

$$\rho = \frac{cov(X,Y)}{\sigma_X \cdot \sigma_Y} = -0.025 \tag{4.5}$$

  where X is the measurement time vector, Y is the transmission time vector, cov is the covariance between X and Y, σ_X is the standard deviation of X and σ_Y is the standard deviation of Y.

  As it is evident there is no clear correlation between the transmission time and the readout delay. This feature can be better seen in Figure 4.12;
- in order to have an overview of the two type of times and of the total time, which is a

time vector given by the sum of the measurement time and readout delay, three histograms with 100 bins have been plotted. In all three cases, the distribution seems multimodal with quantization phenomenon. In particular in Figure 4.13 it is possible to observe that in the 69% of cases approximately, the measurement time is less than 50 ms and the value that appears most frequently is 34.4 ms. Instead, the readout delay (Figure 4.14) is less than 10 ms in the 74% of cases approximately. Finally, the last histogram (Figure 4.15) shows the frequency of occurrence of the total time, that is the time necessary to the teslameter to acquire the measurement and to transmit it. In this case, neglecting the first value, the measurement is always less than 100 ms and the quantization phenomena is more evident, with a repetition of the bell-shaped curves about every 13 ms. This could be due to various reasons such as the scheduling of the processes, the variation of the frequency of the processor, etc. Almost certainly this phenomenon is not due to the teslameter because performing the same program with the creation of only the communication channel and taking the same timestamps by forcing the empty cycles of the same duration of those performed during the test, the phenomenon is still present.

4.3.2 Second Test

The second test was made with a set of 600000 consecutive measurements, in order to have a more meaningful data set to derive statistics. It was performed during the night and lasted about 10 hours.

Field values analysis

The following graph shows the raw field

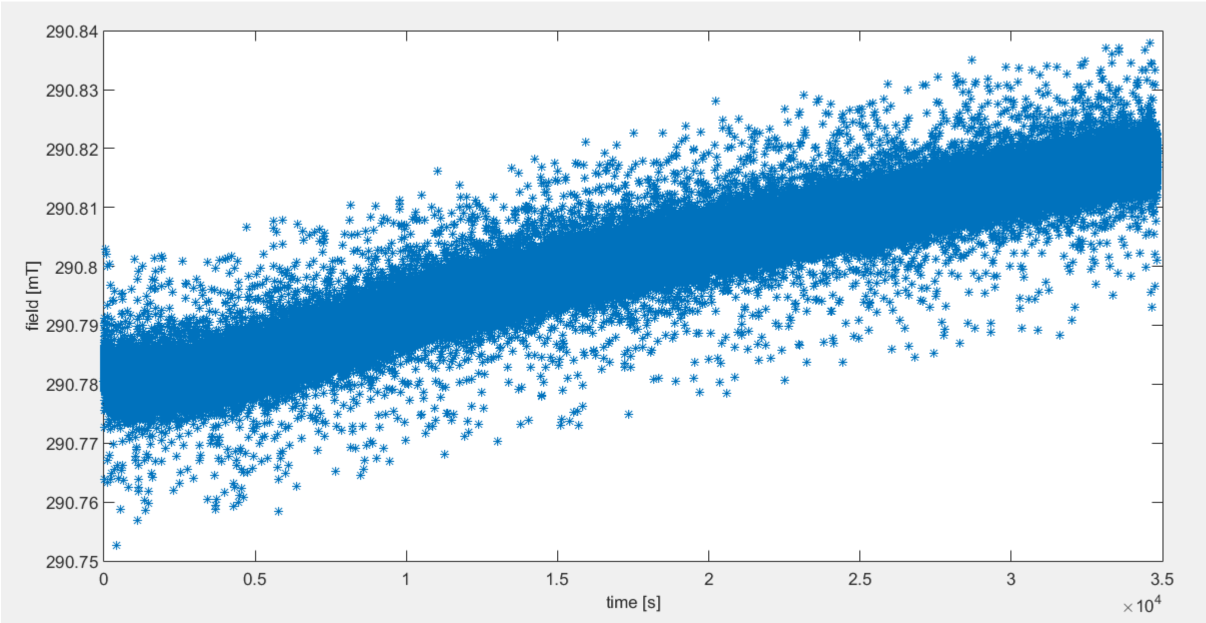

Figure 4.16: Raw field values

Also in this case, the graph shows a trend due to a thermal effect. The relative drift is given by

$$\frac{\text{max value} - \text{min value}}{\text{mean value}} = 292.2 \text{ ppm} \tag{4.6}$$

While in relative terms

$$\frac{292.2}{1200} = 0.24 \text{ °C} \tag{4.7}$$

Therefore we deduce that there was a negative temperature variation lower than 1 °C. In fact, it is interesting to note that the slope in this case is upwards and, as these measurements were made during the night, it is plausible that the temperature was decreasing.

The normalized measurement, obtained by subtracting the drift from the field values, is represented in the following figure

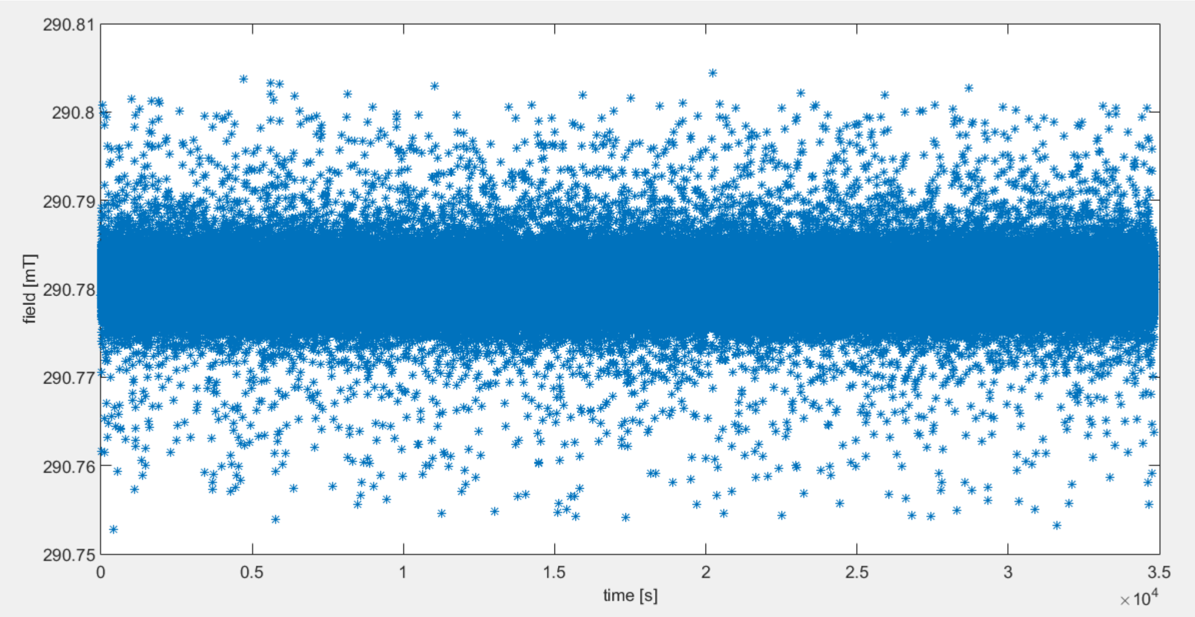

Figure 4.17: Normalized field values

The histogram of the field values is the following

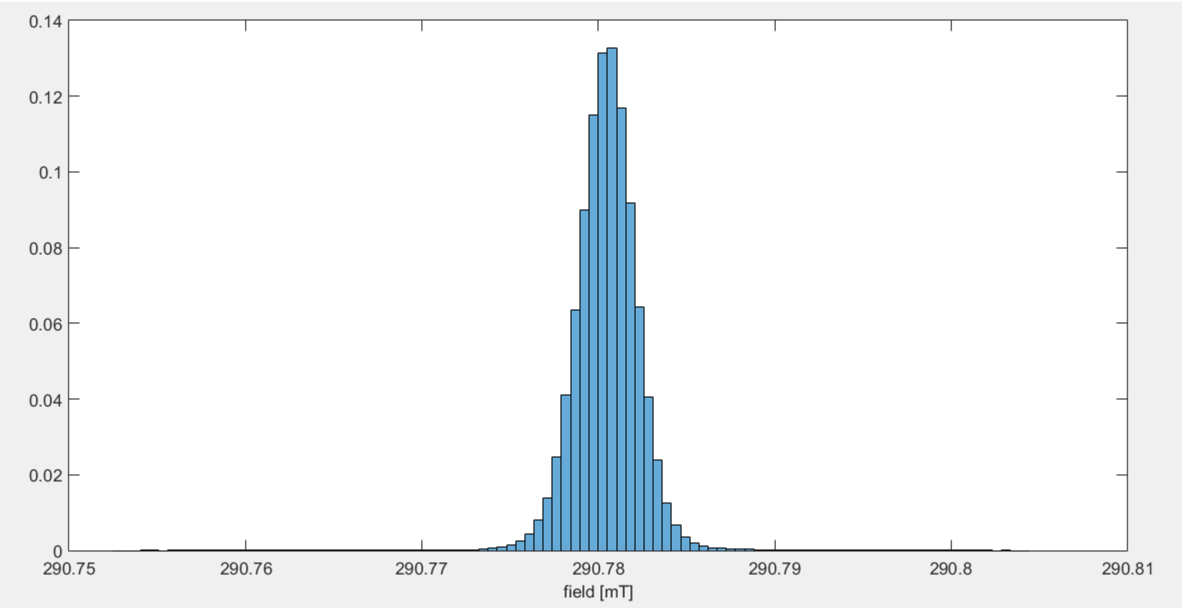

Figure 4.18: Field value histogram

The statistics of the field values are shown in Table 4.5

Parameter	Value [mT]
Mean	290.781
Standard Deviation	$1.835{\times}10^{-3}$
Min	290.753
Max	290.804
Mode	290.78

Table 4.5: Field parameters

The observations made in this case are similar to the observations made for the first test:

- random nature of the noise confirmed by the Gaussian shape (Figure 4.18);
- with reference to the table 4.3, the dispersion of the field values in relative terms is

$$\frac{\text{Standard Deviation}}{\text{Mean}} = \frac{1.835\ \mu\text{T}}{290781\ \mu\text{T}} = 6.31 \cdot 10^{-6} \approx 6 \text{ ppm} \tag{4.8}$$

  this is compatible with the specification of the instrument (±5 ppm [14]);
- the mean field value is compatible with the nominal field of the magnet (Table 4.1).

Timing analysis

As in the case of the first test, two time intervals were also considered in this second experimental test: *measurement time* and *readout delay.*

The graphs showing the experimental results were the following

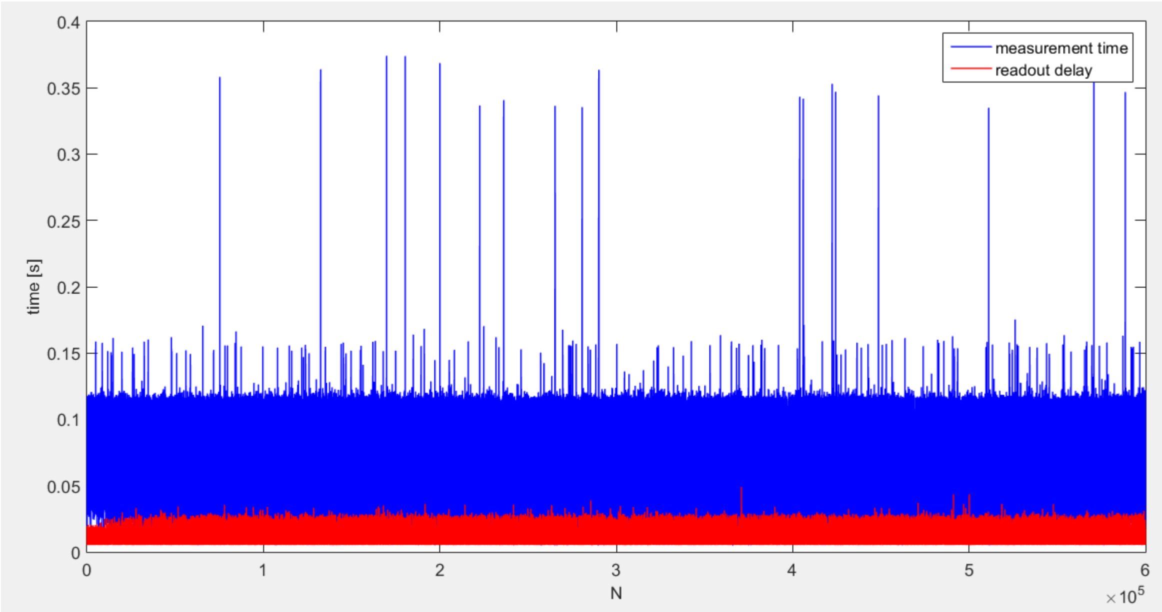

Figure 4.19: Measurement time and readout delay

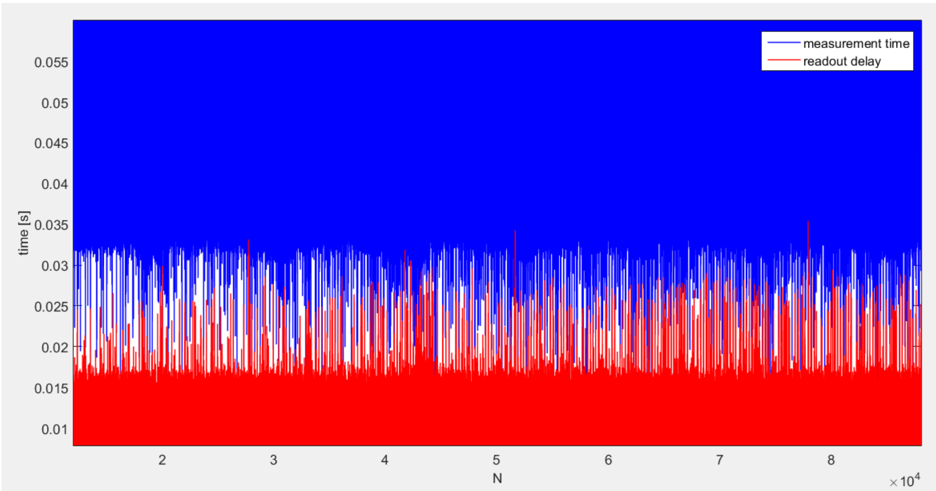

Figure 4.20: Zoom of the previous graph

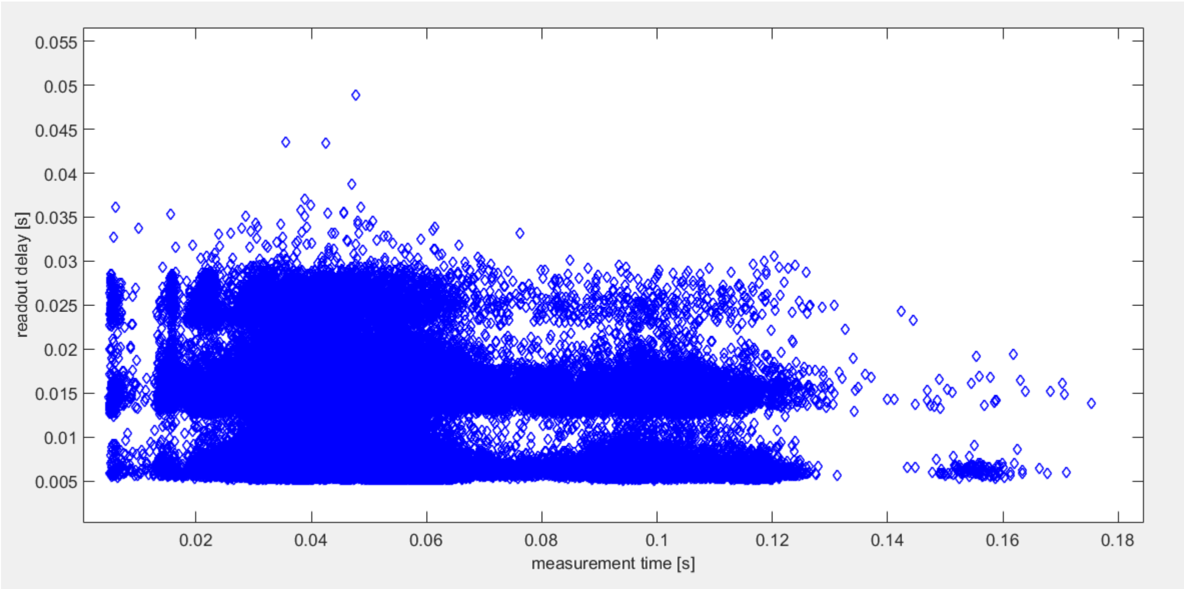

Figure 4.21: Dispersion graph

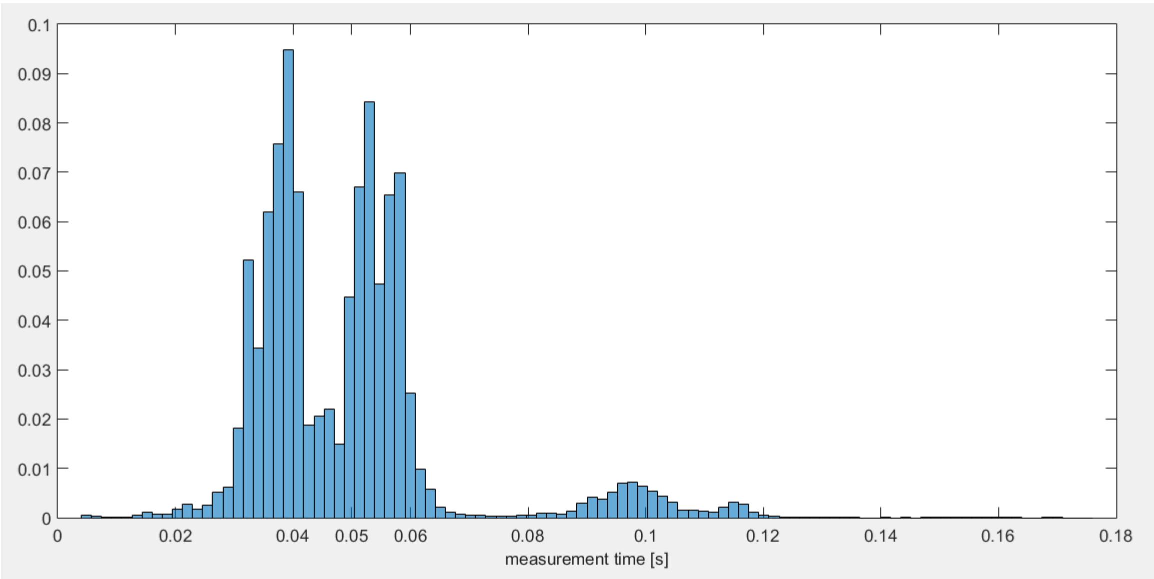

Figure 4.22: Measurement time histogram

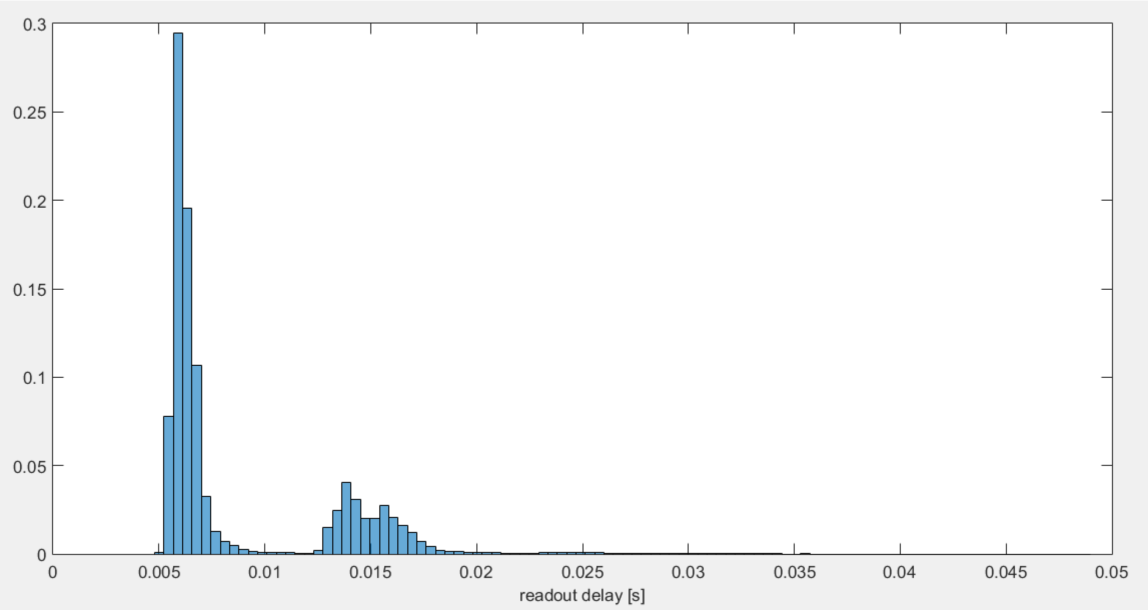

Figure 4.23: Readout delay histogram

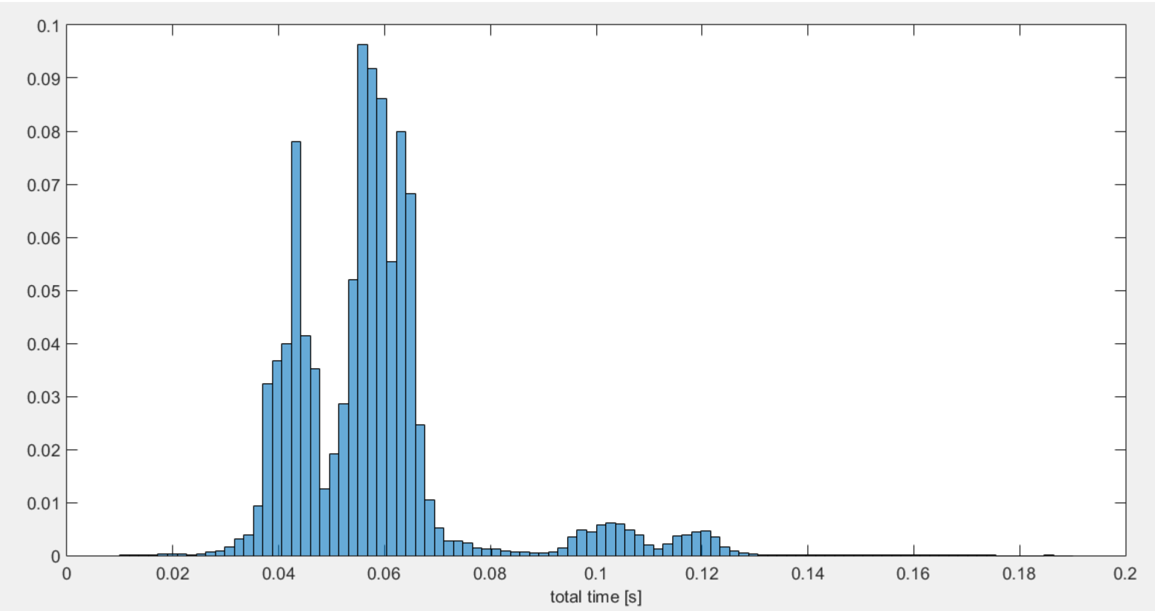

Figure 4.24: Total time histogram

The characteristic parameters for measurement time and readout delay are shown in Table 4.6

Parameter	Measurement time [ms]	Readout delay [ms]	Total time [ms]
Mean	49.4	8.653	58.043
RMS	52.291	9.638	60.464
Standard Deviation	17.149	4.244	16.938
Min	4.818	5.11	10.902
Max	374.14	48.928	189.066
Mode	40.035	5.862	58.182

Table 4.6: Time parameters

Some observations are also made in this case:

- As in the previous case, in Figure 4.19 it is possible to observe that the time required to the readout delay, on average, is less than the time for measurement, as expected;
- in order to verify if there is a correlation between the two parameters (measurement time and readout delay), a correlation coefficient was calculated:

$$\rho = \frac{cov(X,Y)}{\sigma_X \cdot \sigma_Y} = -0.038 \tag{4.9}$$

  where X is the measurement time vector, Y is the transmission time vector, cov is the covariance between X and Y, σ_X is the standard deviation of X and σ_Y is the standard deviation of Y.

  As in the previous test, also in this case there is no clear correlation between the transmission time and the readout delay. This feature can be better seen in Figure 4.21;
- three histograms with 100 bins have been plotted, in order to have an overview of the two type of times and of the total time. In all three cases, the same phenomenon of quantization seen in the case of 10000 experiments, is also present in this other experimental test. In particular in

Figure 4.22 it is possible to observe that in the 56% of cases approximately, the measurement time is less than 50 ms, while in the 93% of cases approximately, the measurement time is less than 60 ms. The value that appears most frequently is 40 ms. Instead, the readout delay (Figure 4.23) is less than 10 ms in the 78% of cases approximately. Finally, the last histogram (Figure 4.24) shows the frequency of occurrence of the total time and, in this case, in the 90% of cases approximately, the measurement is less than 100 ms and the quantization phenomena is less evident than the same plot of the previous test, in the sense that in this case the shape of the bells is not the same for all.

Since the second test observations are almost similar to those of the first test, the second test gives me confidence about the validity of the result.

Chapter 5

Conclusions

5.1 Summary of results

For the analysis made in my thesis among all the sensors we have chosen NMR, for the constant of integration, and the coil, for the part that varies over time. The NMR was chosen because it is the most precise of all. This has been the rational for choice of sensors in a B-Train system and this is an innovation because so far NMR has always been used as a dynamic marker, in my work it will instead be used as a static marker.

Based on the mathematical modeling of the drift and of the results obtained experimentally on ELENA and PSB, combined with the results of the metrological characterization for the NMR, we have analyzed the value of the uncertainty of the field at the end of the next interval, through Equation (2.24), using the new feed-forward correction algorithm and the experimental results of the second test. In both cases, using feed-forward correction is much more advantageous than using correction with static markers only. In fact, in case of correction with static marker, we observe the drift and more time is expected in making the correction plus the error accumulates.

This uncertainty grows linearly, as expected, with the length of the correction interval as shown in Fig. 5.1. The values of the uncertainty of the existing system for the both machine and in case of the new feed-forward correction are given in Table 5.1.

In both machines the RMS value of the voltage offset V_0 is very close, however in the case of ELENA the standard deviation is much smaller than the average, while in the PSB the situation is reversed, that is the fluctuation from one cycle to the next are much more violent and lead even to frequent changes of sign. This makes the impact of the new correction algorithm much more favorable for ELENA.

The target tolerance of 1 μT can be reached by adopting a $T^* \leq 415$ s in ELENA or $T^* \leq 1.2$ s in the PSB. When compared to the RMS uncertainty of the existing measurement, this translates to a potential improvement of a factor about 20 in the PSB but by as much as three orders of magnitude in ELENA. This big difference is due to the much longer plateaux of the ELENA cycle and confirms the validity of the choice of the feed-forward algorithm as the ideal method to be used.

The required period of correction is more than three times longer than the expected length of the ELENA cycle, so therefore potentially only one correction per cycle should be sufficient. For the PSB, we have a T^* of 1.2 s which is also the length of the cycle, so even in this case a correction per cycle is sufficient. In this case it is true that it is necessary to make the correction more frequently but the cycle is also much shorter then, as in ELENA, a correction per cycle is sufficient.

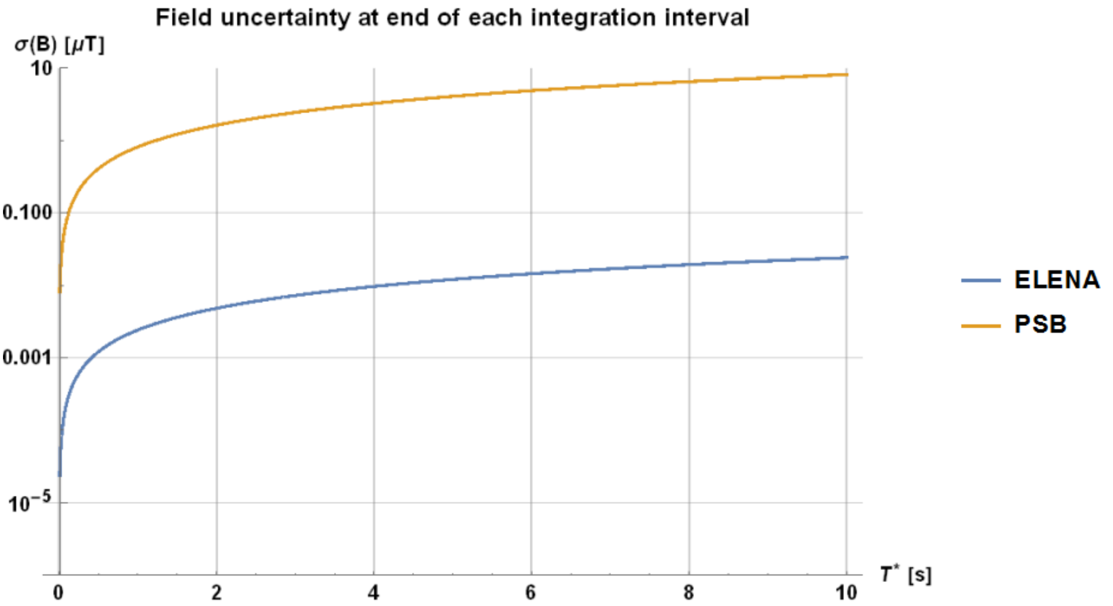

Figure 5.1: Field uncertainty

		Old Correction			New Feed-Forward Correction	
Machine	**Cycle length [s]**	**RMS V_0 [μV]**	**RMS B Drift [μT/s]**	**RMS B error [μT]**	**RMS δV_0 [μV/s]**	**RMS B error (*total*) [μT]**
	Δt	$\sqrt{\langle v_0{}^2\rangle}$	$\frac{1}{A_c}\sqrt{\langle v_0{}^2\rangle}$	$\frac{\Delta t}{A_c}\sqrt{\langle v_0{}^2\rangle}$	$\sqrt{\langle \delta v_{0,k}{}^2\rangle}$	$\sigma\left(B_{mc}(t^*_{k+2})\right)$
ELENA	120	27.7	9.9	**1185.5**	0.2	**1** ($T^* \leq 415$ s)
PSB	1.2	43.5	18.1	**21.7**	57.9	**1** ($T^* \leq 1.2$ s)

Table 5.1: Final results

The main conclusions of this work can be summarized as follows:

- a novel feed-forward drift correction method has been developed analytically and tested using experimental data taken from the existing B-train systems;

- the Metrolab PT2026 NMR teslameter has been tested successfully as a novel kind of quasi-DC field marker with purely software triggering and readout of the field measurement. The results indicate an average latency of 58 ms, which being systematic can be easily taken into account in the correction procedure. The measurement jitter is approximately 17 ms, which gives rise to an error compatible;
- the combination of feed-forward correction and PT2026 as a marker will allow the future B-train systems to meet the very strict specification of 1 μT field stability on long plateaux. In certain cases, this method offers a way to reduce by three orders of magnitude the drift-induced field error with respect to the existing system.

5.1.1 Future work

The future work will consist of implementation of the new feed-forward correction of the drift in the new B-train systems, in particular the FPGA that carries out the real time magnetic flux integration. My own planned contribution will focus on the following aspects:

- exploring alternative, potentially better performing, communication channels with the NMR teslameter. These may include a direct USB connection, or and indirect Ethernet connection through CERN's Technical Network;
- implementing the interface between the teslameter and CERN control system using the FESA framework [27]. This includes building up data structure and functions that could in future be deployed to other magnetic–measurement related frameworks, such as FFMM [28]. It will also be important to define a relevant subset of parameters to be presented to the future users of the interface to configure both the teslameter and the correction algorithm, but also to identify and diagnose fault conditions;
- testing the results of the software developed in the context of the commissioning of the new B-train system, in real-world conditions when the B-train provides feedback to guide and control the beams in all size target accelerators.

Ringraziamenti

I miei ringraziamenti iniziano dalle persone che mi hanno accompagnato durante questi anni universitari, permettendomi di diventare la persona che sono adesso. Prima di tutto un ringraziamento particolare va al mio relatore, il Prof. Pasquale Arpaia, per la sua disponibilità e per avermi incoraggiato ad intraprendere questo percorso di tesi che mi ha portato a trascorrere alcuni bellissimi mesi al CERN, un posto a dir poco stimolante ed entusiasmante.
Vorrei quindi ringraziare tutti i colleghi che ho conosciuto durante il mio periodo di tirocinio a Ginevra, per la loro disponibilità e per avermi fatto sentire accolta fin dal giorno in cui sono arrivata. Un pensiero va al mio supervisore, Marco Buzio, per i suoi preziosi insegnamenti sui campi magnetici e il tempo dedicatomi a spiegarmi materie per me nuove. Ringrazio, inoltre, gli ingegneri di Metrolab per le numerose spiegazioni relative al funzionamento del nuovo teslametro utilizzato durante questo lavoro.

Vorrei spendere due parole speciali di ringraziamento per tutti i fantastici ragazzi che ho conosciuto nella mia sezione, che hanno avuto sempre parole gentili e confortanti, utili a sopportare la nostalgia di casa. In particolare: ringrazio Mariano, per le gite fuori porta e la sua simpatia; Alessandro, Anthony, Carlo, Christian, Ernesto, Joseph, Lucio e Marco R. (un santo), per il loro aiuto e la loro disponibilità; Stefano, Trishna e Vincenzo, per i pranzi e le risate assieme; Gianni, l'Amico che mi mancava.

Ringrazio gli amici di sempre, quelli con cui ho condiviso gli anni dell'università. Iniziando da Daniela, per le ansie condivise prima degli esami e i nostri "tour de force" (come potrebbero capirci gli altri?!): a lei vanno i miei grazie per aver condiviso con me questo e tanto altro; Annalisa, Carmela e Roberta, anche se le nostre strade si sono divise, grazie perchè non sono mancate occasioni per sentirci vicine; ad Aldo, per i progetti fatti insieme e le nostre continue indecisioni; a Catello, Pierpaolo, Vincenzo, Agostino, per il tempo trascorso dentro e fuori l'università. Ringrazio tutti, colleghi e Professori, che mi hanno accompagnato durante questo percorso e aiutato al raggiungimento di questo traguardo, spero di non dimenticare nessuno.

Ringrazio Maria, amica e coinquilina perfetta. Anche se ci conosciamo da più di dieci anni, il nostro affetto è vivo dal primo giorno. Sento di ringraziarla per le pizze, i pomeriggi, le paure e le gioie che abbiamo condiviso. Non avrei mai immaginato che lasciare le quattro mura che ci ha tenuto assieme questi cinque anni, avrebbe aperto in me un vuoto. Questo perchè grazie a lei mi sono sentita sempre a casa.

Ringrazio i miei genitori che mi hanno sempre sostenuto in tanti modi, permettendomi di realizzare i miei sogni. Non hanno mai smesso di credere in me. Li ringrazio per i sacrifici che hanno fatto in questi anni e per essermi stati sempre accanto, spero di poterli riempire d'orgoglio mostrando quella riconoscenza che ogni genitore vorrebbe ricevere e che spesso una figlia non sa dare. Sento di ringraziare mio fratello, perchè mi ha insegnato che nella vita bisogna cogliere al volo i momenti belli che essa ci offre poichè non abbiamo certezza del futuro e affrontare, nonostante tutto, ogni cosa con il sorriso. Ti voglio bene.

Infine, ringrazio Federico per tutto l'amore, la pazienza e il sostegno che mi ha dato durante questo percorso. Grazie per aver creduto in me più di quanto io non riuscissi a fare e per avermi incoraggiato a valicare confini e vincere paure. Se ho svolto una tesi all'estero è certamente anche per merito suo. C'è stata da un lato la voglia di partire e di aprirmi al mondo, dall'altro la paura di non essere all'altezza, oltre che la nostalgia di casa. I suoi consigli mi hanno portato a fare delle scelte che mi hanno permesso oggi di essere qui a farmi fotografare con questa tesi tra le mani. Grazie perchè senza il suo aiuto questa tesi non sarebbe stata mai scritta e oggi foto non ce ne sarebbero state!

A tutti quelli che mi chiedono un consiglio sull'esperienza all'estero, dico "Non abbiate paura di non essere abbastanza, all'inizio può essere difficile, persone che non conosciamo, culture completamente

diverse dalla nostra, nostalgia di casa, ma una volta scalata la montagna, vi assicuro che il panorama è bellissimo". E' stata l'esperienza più bella e importante della mia vita e spero che sia solo un trampolino di lancio per tante altre in futuro. Un giorno mi guarderò indietro e riderò della insicurezza che mi ha assalita prima di partire.

Acknowledgments

My thanks begin with the people who accompanied me during these university years, allowing me to become the person I am now. First of all a special thanks goes to my supervisor, Prof. Pasquale Arpaia, for his availability and for encouraging me to undertake this thesis course that led me to spend some beautiful months at CERN, a stimulating and exciting place. I would therefore like to thank all the colleagues I met during my internship in Geneva, for their availability and for making me feel welcomed since the day I arrived. A special thought goes to my supervisor, Marco Buzio, for his valuable teachings on magnetic fields and the time dedicated to explaining new subjects to me. I also thank the Metrolab engineers for the numerous explanations concerning the operation of the new teslameter used during this work.

I would like to spend two special words of thanks for all the fantastic guys I met in my section, who have always had kind and comforting words, useful to endure homesickness. In particular: I thank Mariano, for trips out of town and his sympathy; Alessandro, Anthony, Carlo, Christian, Ernesto, Joseph, Lucio and Marco R. (a saint), for their help and their availability; Stefano, Trishna and Vincenzo, for lunches and laughter together; Gianni, the friend I needed.

I thank my old friends, those with whom I shared the university years. Starting from Daniela, for the shared anxieties before the exams and our "tour de force" (how can others understand?!): thanks for sharing with me this and much more; Annalisa, Carmela and Roberta, even if we have taken different course of study, thanks because we have always been there for each other; Aldo, for the projects done together and our continuous indecisions; Catello, Pierpaolo, Vincenzo, Agostino, for the time spent inside and outside the university. I thank everyone, colleagues and Professors,

who have accompanied me during this course of study and helped to achieve this final result, I hope I do not forget anyone.

I thank Maria, a friend and a perfect roommate. Although we have known each other for more than ten years, our affection has been alive since the first day. I feel like thanking you for the pizza, the afternoons, the fears and the joys that we shared. I never imagined that leaving the four walls that kept us together these five years would have opened up a void in me. This is because thanks to her I always felt at home.

I thank my parents who have always supported me in many ways, allowing me to realize my dreams. They never stopped believing in me. I thank them for the sacrifices they have made in these years and for being always next to me, I hope I can fill them with pride by showing the gratitude that every parent would like to receive and that often a daughter can not give. I feel like thanking my brother, because he taught me that in life we must seize the beautiful moments that it offers us as we have no certainty of the future and face, despite everything, everything with a smile. I love you.

Finally, I thank Federico for all the love, patience and support he gave me during this period. Thank you for believing in me more than I could and for encouraging me to cross borders and win fears. If I have done a thesis abroad it is certainly also thanks to him. On the one hand there was the desire to leave and open myself to the world, on the other the fear of not being up to the task, as well as the homesickness. His advice led me to make choices that allowed me today to be photographed here with the thesis in my hands. Thanks because without his help this thesis would have never been written and today there would be no photos!

To all those who ask me for advice on the experience abroad, I say "Do not be afraid of not being enough, at first it can be difficult, people we do not know, cultures completely different from ours, homesickness, but once climb the mountain, I assure you that the view is beautiful". It was the most beautiful and important experience of my life and I hope it is only a launching pad for many others in the future. One day I will look back and laugh at the insecurity that attacked me before leaving.

Appendix

Listing 5.1: C program for the communication with the teslameter

```
// Include visa types, functions
#include "visa.h"

#include <stdio.h>
#include <string.h>
#include <time.h>
#include <stdint.h>
#include <sys/timeb.h>
#include <sys/time.h>


/****Function Prototype****/
ViChar *fetch_flux(ViSession, ViSession, ViUInt32, ViStatus);
ViChar *stat(ViSession, ViSession, ViUInt32, ViStatus);


int main()
{
        // Connection info
        ViChar resource_string[] = "TCPIP0::169.254.109.60::inst0::INSTR";
        ViAccessMode access_mode = VI_NULL;
        ViUInt32 timeout_ms = 5000;
```

```
        // Communication buffer
        ViChar buffer1[500];
        ViUInt32 io_bytes;

        ViChar *fetch_value;
        ViChar *stat_op;

        FILE *fd;
        FILE *fd1;
        FILE *fd2;
        FILE *fd3;
        FILE *fd4;



/*********open text file*****************/
fd=fopen("AcquiredTimestampMeasStart.txt", "a");
 if( fd==NULL ) {
    perror("Error_file_opening");
    exit(1);
  }

fd1=fopen("AcquiredFieldValue.txt", "a");
 if( fd1==NULL ) {
    perror("Error_file_opening");
    exit(1);
  }

fd2=fopen("AcquiredTimestampFetch.txt", "a");
 if( fd2==NULL ) {
    perror("Error_file_opening");
    exit(1);
  }
```

```
fd3=fopen("AcquiredTimestampMeasEnd.txt", "a");
 if( fd3==NULL ) {
    perror("Error_file_opening");
    exit(1);
  }

fd4=fopen("numCycles.txt", "a");
 if( fd4==NULL ) {
    perror("Error_file_opening");
    exit(1);
  }

/************ Get VISA resource manager**************/

        ViSession resource_manager;
        ViStatus status;

        status = viOpenDefaultRM(&resource_manager);
        if (status < VI_SUCCESS) {
                printf("Could_not_open_VISA_resource_manager.\n");
                return 0;
        }

/************ Connect to instrument*****************/
        ViSession instrument;

        status = viOpen(resource_manager, resource_string, access_mode, timeout_ms, &instrument);
        if (status < VI_SUCCESS) {
                printf("Error_connecting_to_instrument\n");
                viStatusDesc(resource_manager, status, buffer1);
                printf("%s\n", buffer1);
                return 0;
        }
```

```
/************ Set timeout on instrument ****************/

viSetAttribute(instrument, VI_ATTR_TMO_VALUE, timeout_ms);


/*************** Instrument ID ****************/

idn(instrument, resource_manager, io_bytes, status);


/**************** Set data format *****************/

set_ascii (instrument, resource_manager, io_bytes, status);


/**************** Research of channels with a probe connected *****************/

scan(instrument, resource_manager, io_bytes, status);


/**************** Select channel *****************/

select_channel(instrument, resource_manager, io_bytes, status);


/***************** Model of the probe ********************/

model_probe (instrument, resource_manager, io_bytes, status);


/******************* Start measurement ********************/

start_meas(instrument, resource_manager, io_bytes, status);




long long int j;

int stat_op_int;


for(j = 0; j < 10000; j++){

int i=0;


/******************timestamp in us**************************/

  struct timeval timer_usec;

  long long int timestamp_usec; /* timestamp in microsecond */

  if (!gettimeofday(&timer_usec, NULL)) {

    timestamp_usec = ((long long int) timer_usec.tv_sec) * 1000000ll +

                        (long long int) timer_usec.tv_usec;

  }
```

```
  else {
    timestamp_usec = -1;
  }
  fprintf(fd,"%lld\n", timestamp_usec);
/*************************************************************/

        do{
                stat_op=stat(instrument, resource_manager,io_bytes, status);
                stat_op_int=atoi(stat_op);
                i++;
        }while((stat_op_int & 0x200) == 0);
 fprintf(fd4,"%i\n", i);

/******************timestamp in us***************************/
 long long int timestamp_usec1; /* timestamp in microsecond */
  if (!gettimeofday(&timer_usec, NULL)) {
    timestamp_usec1 = ((long long int) timer_usec.tv_sec) * 1000000ll +
                      (long long int) timer_usec.tv_usec;
  }
  else {
    timestamp_usec1 = -1;
  }
  fprintf(fd3,"%lld\n", timestamp_usec1);

/*********************value collection*********************/
                fetch_value=fetch_flux(instrument, resource_manager, io_bytes, status);
                fprintf(fd1,"%s", fetch_value);

/******************timestamp in us***************************/
 long long int timestamp_usec2;
  if (!gettimeofday(&timer_usec, NULL)) {
    timestamp_usec2 = ((long long int) timer_usec.tv_sec) * 1000000ll +
                      (long long int) timer_usec.tv_usec;
  }
  else {
```

```
    timestamp_usec2 = -1;
  }

 fprintf(fd2,"%lld\n", timestamp_usec2);

}

fclose(fd);
fclose(fd1);
fclose(fd2);
fclose(fd3);
fclose(fd4);

/**************Close down the system***************/
  status = viClose (instrument);
  status = viClose (resource_manager);

  return 0;
}

                              /****Function Definition****/

/*************** check operation status *****************/
ViChar *stat(ViSession instr, ViSession resource_manager, ViUInt32 io_byt, ViStatus status){

        const ViUInt32 Bsize = 1000;
        static ViChar buffer[500];

        ViBuf scpi_command = ":STAT:OPER?";
        status = viWrite(instr, scpi_command, (ViUInt32)strlen(scpi_command), &io_byt);
        if (status < VI_SUCCESS) {
                printf("Error writing to instrument\n");
                viStatusDesc(resource_manager, status, buffer);
```

```
            printf("%s\n", buffer);
            return 0;
        }

        // Read response from instrument
        status = viRead(instr, buffer, Bsize, &io_byt);
        if (status < VI_SUCCESS) {
            printf("Error reading from instrument\n");
            viStatusDesc(resource_manager, status, buffer);
            printf("%s\n", buffer);
            return 0;
        }

        // Response is not null-terminated.
        // Add '\0' at end.
        if (io_byt < Bsize) {
            buffer[io_byt] = '\0';
        }
        else {
            buffer[Bsize] = '\0';
        }

        // Display response
        printf("op_status:\n%s\n\n", buffer);

return buffer;
}

/************** Write *IDN? (id string?)****************/
void idn(ViSession instr, ViSession resource_manager, ViUInt32 io_byt, ViStatus status){

        const ViUInt32 Bsize = 1000;
        ViChar buffer[1000];

        ViBuf scpi_command = "*IDN?";
```

```
    status = viWrite(instr, scpi_command, (ViUInt32)strlen(scpi_command), &io_byt);
    if (status < VI_SUCCESS) {
        printf("Error writing to instrument\n");
        viStatusDesc(resource_manager, status, buffer);
        printf("%s\n", buffer);
        return 0;
    }

    // Read response from instrument
    status = viRead(instr, buffer, Bsize, &io_byt);
    if (status < VI_SUCCESS) {
        printf("Error reading from instrument\n");
        viStatusDesc(resource_manager, status, buffer);
        printf("%s\n", buffer);
        return 0;
    }

    // Response is not null-terminated.
    // Add '\0' at end.
    if (io_byt < Bsize) {
        buffer[io_byt] = '\0';
    }
    else {
        buffer[Bsize] = '\0';
    }

    // Display response
    printf("Instrument id string:\n%s\n\n", buffer);
}

/******** Write :ROUT:PROB:SCAN? (Array of channels which have a probe connected)*******/
void scan(ViSession instr, ViSession resource_manager, ViUInt32 io_byt, ViStatus status){

    const ViUInt32 Bsize = 1000;
    ViChar buffer[1000];
```

```
        ViBuf scpi_command = ":ROUT:PROB:SCAN?";
        status = viWrite(instr, scpi_command, (ViUInt32)strlen(scpi_command), &io_byt);
        if (status < VI_SUCCESS) {
                printf("Error writing to instrument\n");
                viStatusDesc(resource_manager, status, buffer);
                printf("%s\n", buffer);
                return 0;
        }
        // Read response from instrument
        status = viRead(instr, buffer, Bsize, &io_byt);
        if (status < VI_SUCCESS) {
                printf("Error reading from instrument\n");
                viStatusDesc(resource_manager, status, buffer);
                printf("%s\n", buffer);
                return 0;
        }

        // Response is not null-terminated.
        // Add '\0' at end.
        if (io_byt < Bsize) {
                buffer[io_byt] = '\0';
        }
        else {
                buffer[Bsize] = '\0';
        }

        // Display response
        printf("Channels with a probe connected:\n%s\n\n", buffer);
}

/*************** Write :FORM ASC (data format)*****************/
void set_ascii (ViSession instr, ViSession resource_manager, ViUInt32 io_byt, ViStatus status){

        ViChar buffer[1000];
```

```
        ViBuf scpi_command = ":FORM ASC";
        status = viWrite(instr, scpi_command, (ViUInt32)strlen(scpi_command), &io_byt);
        if (status < VI_SUCCESS) {
                printf("Error writing to instrument\n");
                viStatusDesc(resource_manager, status, buffer);
                printf("%s\n", buffer);
                return 0;
        }
}

/*************** Write :ROUT:CLOS (@1) (select channel 1)*****************/
void select_channel(ViSession instr, ViSession resource_manager, ViUInt32 io_byt, ViStatus status){

        ViChar buffer[1000];

        ViBuf scpi_command = ":ROUT:CLOS (@1)";
        status = viWrite(instr, scpi_command, (ViUInt32)strlen(scpi_command), &io_byt);
        if (status < VI_SUCCESS) {
                printf("Error select channel\n");
                viStatusDesc(resource_manager, status, buffer);
                printf("%s\n", buffer);
                return 0;
        }
}

/**************** Write :ROUT:PROB:MOD? (@1) (Model of the probe)********************/
void model_probe (ViSession instr, ViSession resource_manager, ViUInt32 io_byt, ViStatus status){

        ViChar buffer[1000];
        const ViUInt32 Bsize = 1000;

        ViBuf scpi_command = ":ROUT:PROB:MOD? (@1)";
        status = viWrite(instr, scpi_command, (ViUInt32)strlen(scpi_command), &io_byt);
```

```
        if (status < VI_SUCCESS) {
                printf("Error writing to instrument\n");
                viStatusDesc(resource_manager, status, buffer);
                printf("%s\n", buffer);
                return 0;
        }

        // Read response from instrument
        status = viRead(instr, buffer, Bsize, &io_byt);
        if (status < VI_SUCCESS) {
                printf("Error reading from instrument\n");
                viStatusDesc(resource_manager, status, buffer);
                printf("%s\n", buffer);
                return 0;
        }

        // Response is not null-terminated.
        // Add '\0' at end.
        if (io_byt < Bsize) {
                buffer[io_byt] = '\0';
        }
        else {
                buffer[Bsize] = '\0';
        }

        // Display response
        printf("Model of the probe:\n%s\n\n", buffer);
}

/****************** Write :INIT:CONT 1 (Start measurement)*********************/
void start_meas(ViSession instr, ViSession resource_manager, ViUInt32 io_byt, ViStatus status){

        ViChar buffer[1000];

        ViBuf scpi_command = ":INIT:CONT 1";
```

```
        status = viWrite(instr, scpi_command, (ViUInt32)strlen(scpi_command), &io_byt);
        if (status < VI_SUCCESS) {
                printf("Error␣select␣channel\n");
                viStatusDesc(resource_manager, status, buffer);
                printf("%s\n", buffer);
                return 0;
        }
}

/************** Write :FETC:SCAL:FLUX? (Measured flux density)************************/
ViChar *fetch_flux(ViSession instr, ViSession resource_manager, ViUInt32 io_byt, ViStatus status){

        ViChar buffer[2000];
        const ViUInt32 Bsize = 1000;

        ViBuf scpi_command = ":FETC:SCAL:FLUX?";
        status = viWrite(instr, scpi_command, (ViUInt32)strlen(scpi_command), &io_byt);
        if (status < VI_SUCCESS) {
                printf("Error␣writing␣to␣instrument\n");
                viStatusDesc(resource_manager, status, buffer);
                printf("%s\n", buffer);
                return 0;
        }

        // Read response from instrument
        status = viRead(instr, buffer, Bsize, &io_byt);
        if (status < VI_SUCCESS) {
                printf("Error␣reading␣from␣instrument\n");
                viStatusDesc(resource_manager, status, buffer);
                printf("%s\n", buffer);
                return 0;
        }
```

```
        // Response is not null−terminated.
        // Add '\0' at end.
        if (io_byt < Bsize) {
                buffer[io_byt] = '\0';
        }
        else {
                buffer[Bsize] = '\0';
        }
 return buffer;
}
```

Bibliography

[1] M. Di Castro, D. Sernelius, L. Bottura, L. Deniau, N. Sammut, S. Sanfilippo, W. Venturini Delsolaro, “Parametric field modeling for the LHC main magnets in operating conditions”, Proceedings of PAC07, Albuquerque, New Mexico, USA

[2] M. Buzio, “Real-time field control and measurement”, International Master of Hadronteraphy, CNAO, Pavia (IT), 2013

[3] Stéphane Deghaye, Eve Fortescue-Beck, “Introduction to the BE/CO control system” 2016 Edition – Part 1

[4] F. M. Velotti, W. Bartmann, T. Bohl, C. Bracco, K. Cornelis, M. A. Fraser, B. Goddard, V. Kain, L. S. Stoel, CERN, Geneva, Switzerland, “Characterisation of the SPS slow-extraction parameters”, Proceedings of IPAC2016, Busan, Korea

[5] https://home.cern/about/experiments/alpha

[6] https://home.cern/about/experiments/asacusa

[7] https://home.cern/about/experiments/atrap

[8] https://home.cern/about/experiments/base

[9] M. Pezzetta, G. Bazzano, E. Bressi, L. Falbo, M. Pullia, C. Priano, CNAO Foundation, Pavia, Italy, G. Venchi, University of Pavia, Italy, O. Coiro, G. Franzini, D. Pellegrini, M. Serio, A. Stella, LNF-INFN, Frascati, Italy, “B-Train performances at CNAO”, Proceedings of IPAC2011, San Sebastián, Spain

[10] P.Arpaia, M. Buzio, F. Caspers, G. Golluccio, C. Petrone, Department of Engineering, University of Sannio, CERN - European Organization for Nuclear Research, "Static Metrological Characterization of a Ferrimagnetic Resonance Transducer for Real-Time Magnetic Field Markers in Particle Accelerators"

[11] D. Cornuet, "B-trains for the particle accelerators", AT-MTM Technical Seminar, 2007

[12] M. Buzio, "The B-train system", ELENA Design Report, Chapter 4.10

[13] Joseph M. Kelly, "Magnetic Field Measurement with Peaking Strips", Brookhaven National Laboratory, The review of scientific instruments, Vol 22 number 4, 1951

[14] Metrolab, NMR Precision Teslameter PT2026 - User's Manual, version 1.3

[15] Yanli Yang, Yanfei Zhao, School of Electronics and Information Engineering, Tianjin Polytechnic University, Tianjin, China, Dali Kang, Dalian ShengLiLai Monitoring Technology Co., Ltd., Dalian 116031, China, "Integration on acceleration signals by adjusting with envelopes", Journal of Measurements in Engineering, Vol. 4, Issue 2, 2016, p. 117-121

[16] Tiago Ferreira de Castro te Lintel Hekkert, Instituto de Plasmas e Fusão Nuclear (IPFN) Instituto Superior Técnico - IST, Universidade de Lisboa - UL, Av. Rovisco Pais 1, 1049-001 Lisbon, Portugal, October 2013, "Data Acquisition and Digital Processing in Nuclear Fusion"

[17] D. M. Liu, W. Z. Zhao, Y. G. He, B. Chen, School of Electrical Engineering and Automation, Hefei University of Technology, Hefei 230009, China, B. N. Wan, B. Shen, J. Huang, H. Q. Liu, Institute of Plasma Physics, Chinese Academy of Sciences, Hefei 230031, China, "Development of an alternating integrator for magnetic measurements for experimental advanced superconducting tokamak", Review of Scientific Instruments 85, 11E826 (2014)

[18] J. G. Bak, S. G. Lee, the KSTAR Project Team, Korea Basic Science Institute, Yusung, Taejeon 305-806, Korea, and DeRac Son, Department of Physics, Hannam University, Taejeon 306-791, Korea, Rev. Sci. Instrum., "Performance of the magnetic sensor and the integrator for the KSTAR magnetic diagnostics"

[19] Seong-Heon Seo, National Fusion Research Institute, Daejeon 305-333, Korea Andreas Werner, and M. Marquardt,Max-Planck Institut fuer Plasmaphysik, Wendelsteinstrasse 17491 Greifswald, Germany, "Development of a digital integrator for the KSTAR device", Rev Sci Instrum. 2010 Dec

[20] S. Ali-Arshad and L. de Kock, JET Joint Undertaking, Abingdon Oxon OX14 3EA, United Kingdom, Rev. Sci. Instrum., "Long-pulse analog integration"

[21] E. J. Strait, J. D. Broesch, R. T. Snider, and M. L. Walker, General Atomics, San Diego, California 92186-9784, "A hybrid digital–analog long pulse integrator"

[22] Chen, C., Fan, WW., Pan, YH. et al., NUCL SCI TECH (2016), "A multi-channel real-time digital integrator for magnetic diagnostics in HL-2A tokamak"

[23] P. Arpaia, P. Cimmino, L. Fiscarelli, European Organization for Nuclear Research (CERN), Geneva, Switzerland and University of Sannio, Department of Engineering, L. De Vito, University of Sannio, Department of Engineering, "Offset correction in a digital integrator for rotating coil measurements", XX IMEKO World Congress, Metrology for Green Growth, September 9−14, 2012, Busan, Republic of Korea

[24] http://www.ivifoundation.org/docs/scpi-99.pdf

[25] https://www.centos.org/

[26] https://www.ni.com/visa/

[27] Michel Arruat, Leandro Fernandez, Stephen Jackson, Frank Locci, Jean-Luc Nougaret, Maciej Peryt, Anastasiya Radeva, Maciej Sobczak, Marc Vanden Eynden, Accelerators and Beams Department, CERN, Geneva, Switzerland, "Front-End Software Architecture", Proceedings of ICALEPCS07, Knoxville, Tennessee, USA

[28] P. Arpaia, Department of Engineering, Universityof Sannio, L. Bottura, CERN, Dept. AT (Accelerator Technology), Group MTM, V. Inglese, G. Spiezia, Department of Engineering, University of Naples - Federico II, "A flexible software framework for magnetic measurements at CERN: a prototype for the new generation of rotating coils"